MINISTRY OF EDUCATION

THE ANNALS OF "DUNAREA DE JOS" UNIVERSITY OF GALATI

Fascicle IX
METALLURGY AND MATERIALS SCIENCE

YEAR XL (XLV)
September 2022, no. 3

ISSN 2668-4748; e-ISSN 2668-4756

2022
GALATI UNIVERSITY PRESS

EDITORIAL BOARD

THE ANNALS OF "DUNAREA DE JOS" UNIVERSITY OF GALATI
FASCICLE IX. METALLURGY AND MATERIALS SCIENCE
Nº. 3 - 2022, ISSN 2668-4748; e-ISSN 2668-4756
Volume DOI: https://doi.org/10.35219/mms.2022.3

Table of Contents

THE ANNALS OF "DUNAREA DE JOS" UNIVERSITY OF GALATI
FASCICLE IX. METALLURGY AND MATERIALS SCIENCE
Nº. 3 - 2022, ISSN 2668-4748; e-ISSN 2668-4756
Volume DOI: https://doi.org/10.35219/mms.2022.3

THE ANNALS OF "DUNAREA DE JOS" UNIVERSITY OF GALATI
FASCICLE IX. METALLURGY AND MATERIALS SCIENCE
No. 3 - 2022, ISSN 2668-4748; e-ISSN 2668-4756
Article DOI: https://doi.org/10.35219/mms.2022.3.01

EFFECT OF THE TEMPERATURE AND OXIDATION TIME ON SOME PHYSICOCHEMICAL CHARACTERISTICS OF THE RICE BRAN OIL

Romică CREȚU, Liviu Cătălin ȘOLEA
"Dunarea de Jos" University of Galati, Romania
e-mail: romy_cretu@yahoo.com

ABSTRACT

Due to their excellent characteristics, vegetable oils are successfully used in various formulations of organic lubricants. In this context, the advanced biodegradability and excellent lubricity performance of rice oil leads to its being considered as a real potential for the lubricants industry. However, as with other vegetable oils, the stability of rice bran oil is strongly influenced by the oxidation process. Therefore, the aim of this work was the oxidation stability monitorization of rice bran oil by spectrophotometric techniques. For this purpose, oxidation tests of rice bran oil at elevated temperatures were performed.

In this paper, transmittance spectra were determined, and the trichromatic components and coordinates were calculated, as well as the colour differences for rice oils subjected to a forced oxidation treatment at temperatures of 100 °C and 120 °C for 4, 8 and 10 hours. The results obtained show that, although after the first 4 hours of forced oxidation significant changes appear on the physicochemical properties of rice bran oil, an increase in the test time from 8 to 10 hours does not lead to significant changes in the analysed parameters, the conclusion being valid for both test temperatures.

KEYWORDS: rice bran oil, oxidation, transmittance, eco-friendly lubricant

1. Introduction

Rice (Oryza Sativa L.) is considered the oldest cultivated plant; it began to be cultivated 8000 years ago in South Asia while in Europe it was first cultivated around the 8th century especially in Spain. In Romania, the first rice plantation dates to the 18th century and was cultivated in the Banat area [1].

Rice is the world's third most important cereal in terms of annual production, but the most important food crop in terms of caloric and nutritional value. In 2019, world's leading rice producers were: China - 148 million tons and India - 116 million tons, while in Romania rice production was 40,000 tons [2]. About two-thirds of the rice consumed by Europeans is grown in the EU, the rest is imported from India or Cambodia.

Rice bran oil is obtained by cold pressing the husk of the rice grain, followed by extraction and refining for dewaxing and deodorization. Rice bran oil contains saturated and unsaturated fatty acids as well as a number of bioactive compounds such as gamma-oryzanol, tocotrienols and tocopherols [3, 4].

Rice bran oil can also be used as an edible oil in recent times and as a raw material to produce bio-fuels and environmentally friendly lubricants [5-11]. Recently, a series of tribological and rheological studies have been conducted on rice bran oils [12-19]. The study of rice bran oil has been addressed by a number of researchers, among whom we can mention [20-23].

2. Experimental Details

In this paper, transmittance curves were determined for rice bran oils subjected to a forced oxidation treatment at temperatures of 100 °C and 120 °C, for 4, 8 and 10 hours, maintaining a constant flow of 29 L/min of air. The transmittances of the oxidized samples as well as the non-oxidized oil with the T60 spectrophotometer, produced by PG Instruments Limited (C.E.) were determined. The transmittance values in the wavelength range of 380 - 780 nm were determined.

Also, from spectral transmittance curves, the samples for colour in the x, y, z or L^*, a^*, b^* and

THE ANNALS OF "DUNAREA DE JOS" UNIVERSITY OF GALATI
FASCICLE IX. METALLURGY AND MATERIALS SCIENCE
No. 3 - 2022, ISSN 2668-4748; e-ISSN 2668-4756
Article DOI: https://doi.org/10.35219/mms.2022.3.01

C^*_{ab}, h_{ab} coordinates: CIEXYZ, CIE $L^*a^*b^*$ (CIELAB) and CIE $L^*C^*_{ab}{}^*h_{ab}$ (CIELCH) colour systems were measured. CIE $L^*a^*b^*$ scale is recommended by Commission Internationale de l'Eclairage [24]. Illumination was performed by D65/10°. Furthermore, the rice oil colour differences were calculated.

3. Experimental Results

Figures 1-5 show the transmittance curves of oxidized oils at temperatures of 100 ºC and 120 ºC for 4, 8 and 10 hours as well as for non-oxidized oil. Based on the experimental values of the transmittances determined at wavelengths of 445, 495, 550 and 625 nm, trichromatic components and coordinates were calculated (Tables 1 and 4), these being the calculation support for determining the chromatic coordinates (Tables 2 and 5) and colour differences (Tables 3 and 6) for the oxidized oils at temperatures of 100 ºC and 120 ºC for 4, 8 and 10 hours as well as for non-oxidized oil.

Figure 1 shows the transmittance curves of non-oxidized and oxidized oil for 4, 8 and 10 hours at 100 °C. Analysing the transmittance curves, it is observed that in the wavelength range between 380-470 nm there are no differences in the transmittance values between non-oxidized oil and oxidized oil for 4 hours. However, after 470 nm, due to oxidative degradation, under the action of O_2 from the bubbled air in the rice oil samples, through radical chain reactions [25], noticeable differences in transmittance spectra appear.

Increasing the exposure time to forced oxidation to 8 and 10 hours, respectively, over the entire wavelength range analysed, major differences in transmittance values appear compared to non-oxidized oil.

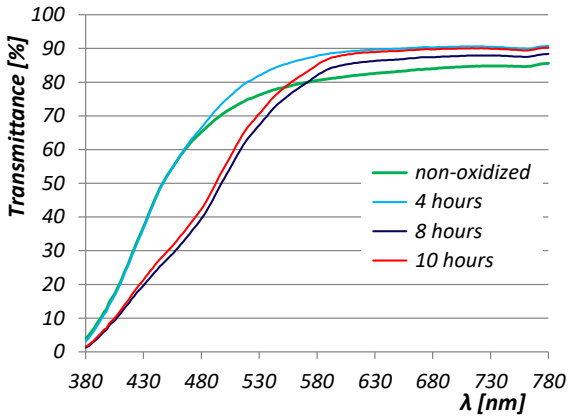

Fig. 1. *Spectral transmittance curves of oxidized rice oils at 100 °C for 4, 8 and 10 hours*

Comparing the oxidized oils for 8 and 10 hours, there are no major differences in the values of their transmittance. Both oils show, in the first half of the wavelength range, decreases in transmittances compared to non-oxidized oil, due to the oxidation of lipids present in the composition of rice oil, most likely caused by the presence of molecular oxygen. Subsequently, according to the results shown in figure 1, there are increases in transmittance in the last part of the studied interval. Moreover, performing the oxidation test at a higher temperature, respectively increasing the oxidation temperature to 120 °C, causes significant changes in the transmittance spectra of oxidized oils 4, 8 and 10 hours compared to non-oxidized oil (Fig. 2).

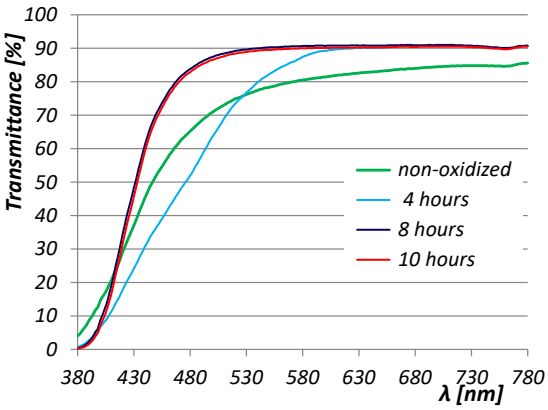

Fig. 2. *Spectral transmittance curves of oxidized rice oils at 120 °C for 4, 8 and 10 hours*

These changes have the probable cause that oxygen and the unsaturated substrate are potential generators of free radicals, a property that accentuates the temperature increase by 20 degrees. In this context, there is a decrease in the transmittance of the analysed sample to about 520 nm due to the increase in the degree of absorption. In addition, after this inflection point, due to the decomposition of hydroperoxides formed by excessive oxidation, there is a decrease in the degree of absorption. The same positive variation is also observed for the oxidation of rice oil samples for 8 hours and 10 hours. Between the latter, no noticeable differences in the variation of the transmittance spectra are found.

These results show that increasing the temperature to 120 °C for up to 8 hours leads to a maximum degree of oxidation of rice oil under the conditions of the experiment. It appears that after this time, the variation of the transmittance spectra is similar. All these findings presented above are also highlighted in Figures 3-5.

According to the obtained results, it is noted that at least in the second part of the transmittance spectra (after 580 nm) the oxidation of the oil samples at the

THE ANNALS OF "DUNAREA DE JOS" UNIVERSITY OF GALATI
FASCICLE IX. METALLURGY AND MATERIALS SCIENCE
No. 3 - 2022, ISSN 2668-4748; e-ISSN 2668-4756
Article DOI: https://doi.org/10.35219/mms.2022.3.01

highest temperature under the experimental conditions (120 °C) led to more accelerated transformations of monounsaturated fatty acids (C18: 1, over 41%) and polyunsaturated (C18: 2, over 30%) (the results not shown) in the composition of the studied oil. However, it is highlighted (Figure 3, Tables 2 and 5) the hypsochromic displacement in the first stage of oxidation of the oil samples, when there is also a colour change induced by the selective transmission of light.

All these changes in physicochemical properties due to the oxidation process can lead to a drastic change in lubrication performance, in the context of which this oil can be considered a potential eco-friendly lubricant.

Moreover, the oxidation of the oils was revealed by determining the chromatic parameters. Comparing the chromatic parameters calculated for each oxidized oil at a temperature of 100 ºC and the oxidation periods of 4, 8 and 10 hours, it is observed the increase of the brightness parameter (L^*) after 4 hours of oxidation by 2.93%. In addition, when the process of forced oxidation is continued, there is a decrease of about 3% of this parameter after 8 hours of oxidation. Although there is a slight increase after 10 hours of oxidation, this chromatic parameter still shows a decrease compared to the sample of non-oxidized oil (Table 2). Thus, after 10 hours of oxidation, the brightness decreases by 1.38% compared to non-oxidized oil.

On the other hand, if after the first 4 hours of oxidation at 120 ºC the increase in brightness is insignificant, our results show that the increase in oxidation temperature causes, after 8 hours of oxidation, an increase in the brightness parameter by 5.8% compared to the control sample.

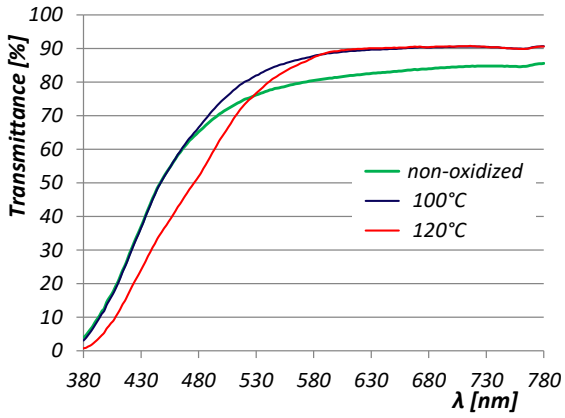

Fig. 3. *Spectral transmittance curves of oxidized rice oils for 4 hours at 100 °C and 120 °C*

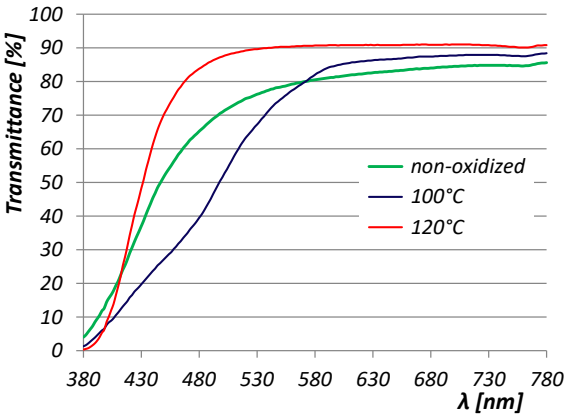

Fig. 4. *Spectral transmittance curves of oxidized rice oils for 8 hours at 100 °C and 120 °C*

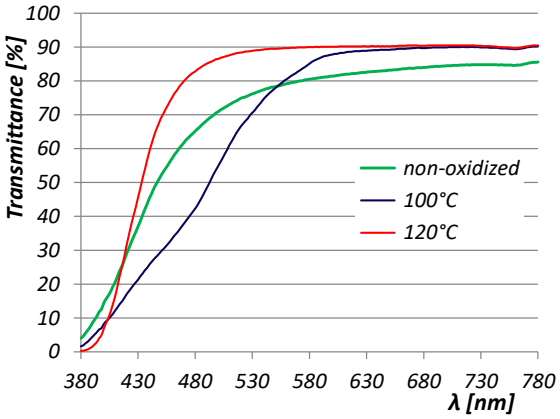

Fig. 5. *Spectral transmittance curves of oxidized rice oils for 10 hours at 100 °C and 120 °C*

Likewise, the continuation of the forced oxidation up to 10 hours led to an increase in brightness by over 5%, although in this case there is a slight decrease compared to the previous stage of the study (Table 5).

The yellowness parameter (b^*) for oxidized oils at 100 ºC has a slight tendency to increase after 4 hours of oxidation, followed by a significant increase after 8 hours of oxidation, while after 10 hours of oxidation this parameter records an exceedingly small decrease compared to the previous oxidation (Table 2).

The increase in oxidation temperature from 100 °C to 120 °C causes a significant increase after 4 hours (approximately 125%), followed by a significant decrease after 8 hours of oxidation. There is then an insignificant increase in this parameter in the case of oxidized oil for 10 hours compared to oxidized oil for 8 hours (Table 5). This suggests that, after the first 4 hours of oxidation, the rice oil is much more exposed to the change in the CIE value b^*. The yellowness parameter was, however, the most

THE ANNALS OF "DUNAREA DE JOS" UNIVERSITY OF GALATI
FASCICLE IX. METALLURGY AND MATERIALS SCIENCE
No. 3 - 2022, ISSN 2668-4748; e-ISSN 2668-4756
Article DOI: https://doi.org/10.35219/mms.2022.3.01

noticeable change from a visual point of view. If in the case of oil samples subjected to oxidation at 100 °C the difference in yellow degree shows that they become yellower than the control sample regardless of the degree of oxidation (Tables 3 and 6), our results show that when oxidation is performed at 120 °C this has place only after oxidation for 4 hours.

In this case, after oxidation of the oil samples for 8 and 10 hours, respectively, it is found that they become less yellow (Table 6).

The results of this study indicated strong correlations of yellowness parameter with C_{ab}* chroma, as well as with the angle of the shade, h_{ab}. Thus, from Table 2 and Table 5 the colour variation of the analysed oil can be noticed within the first quadrant of the chromatic circle, regardless of whether the study was performed at 100 °C or 120 °C. This means that although the other chromatic parameters confirm obvious colour changes depending on the oxidation conditions, however these changes do not pass from one dial to another in the chromatic circle.

In this respect, the degree of oxidation can also be highlighted by comparing the colour differences (ΔE^*ab) recorded between the oxidized samples and the non-oxidized reference samples (Fig. 6).

Oxidized oil at 100 ºC for 4 hours, although it produces or differs slightly, this is clearly seen. Increasing the oxidation time to 8 hours shows a sharp increase in colour differences, the oil undergoes an intense oxidation process, it is maintained after 10 hours of oxidation, the colour difference has a high value, but slightly less than that recorded in the case of oxidized oil 8 hours. In both cases, namely oxidation at 8 and 10 hours, the results obtained show distinct colours for the observer in the case of the analysed samples.

Increasing the test temperature to 120 ºC the highest value of colour differences is recorded after 4 hours of testing, this indicating an accentuated oxidation process, followed by lower values of this parameter for oxidized oils for 8 and 10 hours.

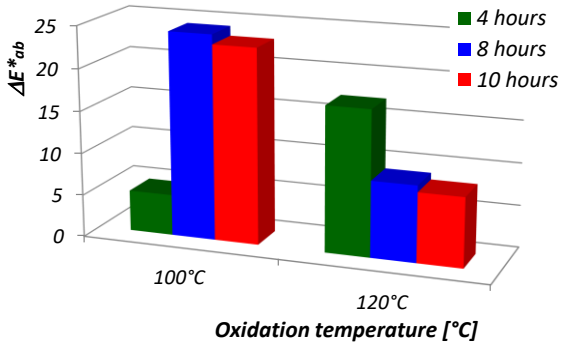

Fig. 6. *Colour differences (ΔE^*_{ab}) for oxidized rice oils*

Table 1. *Experimental results for rice oils oxidized at a temperature of 100 °C, obtained according to the colour system (x, y) CIE 1964 (CIEXYZ)/iluminant D65/10°*

Rice oils 100 °C	Trichromatic components			Trichromatic coordinates		
	X	Y	Z	x	y	z
Non-oxidized	72.324	74.149	62.775	0.346	0.354	0.300
4 hours oxidized	77.634	79.811	63.249	0.352	0.362	0.287
8 hours oxidized	67.669	68.580	35.692	0.394	0.399	0.208
10 hours oxidized	70.410	71.565	38.493	0.390	0.397	0.213

Table 2. *Chromatic coordinates (systems: CIELAB) for rice oils oxidized at 100 °C/ Iluminant D65/10°*

Rice oils 100 °C	Chromatic coordinates			a^*/b^*	$(a^*/b^*)^2$	C^*_{ab}	h_{ab}
	L^*	a^*	b^*				
Non-oxidized	88.99	4.30	13.75	0.31	0.10	14.41	72.64
4 hours oxidized	91.60	3.98	17.83	0.22	0.05	18.26	77.42
8 hours oxidized	86.30	5.91	37.80	0.16	0.0244	38.26	81.13
10 hours oxidized	87.76	5.55	36.79	0.15	0.023	37.20	81.42

Table 3. *Experimental values of colour differences for rice oils oxidized at 100 °C*

Rice oils 100 °C	ΔL^*	Δa^*	Δb^*	ΔC^*_{ab}	Δh_{ab}	ΔE^*_{ab}
4 hours oxidized	2.61	-0.32	4.08	3.86	4.78	4.85
8 hours oxidized	-2.70	1.61	24.05	23.85	8.48	24.25
10 hours oxidized	-1.23	1.25	23.04	22.80	8.78	23.10

THE ANNALS OF "DUNAREA DE JOS" UNIVERSITY OF GALATI
FASCICLE IX. METALLURGY AND MATERIALS SCIENCE
No. 3 - 2022, ISSN 2668-4748; e-ISSN 2668-4756
Article DOI: https://doi.org/10.35219/mms.2022.3.01

Table 4. *Experimental results for rice oils oxidized at a temperature of 120 °C, obtained according to the colour system (x, y) CIE 1964 (CIEXYZ)/iluminant D65/10°*

Rice oils 120 °C	Trichromatic components			Trichromatic coordinates		
	X	Y	Z	x	y	z
Non-oxidized	72.324	74.149	62.776	0.346	0.354	0.300
4 hours oxidized	73.679	75.541	46.387	0.368	0.400	0.232
8 hours oxidized	83.727	86.364	83.330	0.330	0.341	0.329
10 hours oxidized	82.807	85.433	81.469	0.332	0.342	0.326

Table 5. *Chromatic coordinates (systems: CIELAB) for rice oils oxidized at 120 °C/ Iluminant D65/10°*

Rice oils 120 °C	Chromatic coordinates			a^*/b^*	$(a^*/b^*)^2$	C^*_{ab}	h_{ab}
	L^*	a^*	b^*				
Non-oxidized	88.99	4.30	13.75	0.31	0.10	14.41	72.64
4 hours oxidized	89.65	4.32	30.92	0.14	0.02	31.22	82.05
8 hours oxidized	94.47	3.55	6.63	0.54	0.29	7.52	61.84
10 hours oxidized	94.07	3.50	7.32	0.48	0.23	8.11	64.43

Table 6. *Experimental values of colour differences for rice oils oxidized at 120 °C*

Rice oils 120 °C	ΔL^*	Δa^*	Δb^*	ΔC^*_{ab}	Δh_{ab}	ΔE^*_{ab}
4 hours oxidized	0.65	0.02	17.17	16.82	9.41	17.18
8 hours oxidized	5.47	-0.75	-7.12	-6.89	-10.80	9.01
10 hours oxidized	5.08	-0.80	-6.43	-6.29	-8.21	8.23

4. Conclusions

The rice bran oil was subjected to forced oxidation treatments at temperatures of 100 °C and 120 °C, the oxidation times being 4, 8 and 10 hours. The transmittance curves of the oxidized samples were determined and the trichromatic components and coordinates, chromatic coordinates and colour differences were calculated.

The present study showed that for oxidized oil for 10 hours at 100 °C, the brightness parameter (L^*) decreases by 1.4% compared to non-oxidized oil, while for oxidized oil at 120 °C this parameter increases by 5.7%. The yellowness parameter (yellow component b^*) was the most noticeable change visually. The yellowness parameter, in the case of oxidized oil for 10 hours at 100 °C, increases by 168% compared to non-oxidized oil, while for oxidized oils at 120 °C the increase occurs only in the first 4 oxidation hours. In the case of oxidation at 120 °C this parameter decreases throughout the oxidation set in this study by 76.7%.

The largest increases in colour differences were recorded in the case of oils tested at 100 °C for 8 to 10 hours. However, increasing the test temperature from 100 °C to 120 °C for oxidized oils for 4 hours results in a sharp increase in the colour difference. For oils tested at 120 °C, a significant increase in colour difference is observed after 4 hours of testing, followed by a significant decrease for both 8 and 10 hours.

Thus, the results obtained show that, although after the first 4 hours of forced oxidation there are significant changes in the physicochemical properties of rice oil, an increase in test time from 8 to 10 hours does not lead to significant changes in the analysed parameters, the conclusion being valid for both test temperatures.

References

[1]. ***, www.risoscotti.r/ro/istoria-orezului.
[2]. ***, https://agriportal.ro/stiri/focus/productia-de-orez-in-2019-145. htm.
[3]. Preuk T., Sutsawat D., Attasak Jaree., *Development of separation method for Alpha-Tocopherol and Gamma-Oryzanol extracted from rice bran oil using Three-Zone simulated moving bed process*, Separation and Purification Technology, 272, 118930, 2021.
[4]. Ruru L., Ying X., Ming C., Lin T., Mengyao L., Ruijie L., Qingzhe J., Xingguo W., *Antioxidant interaction of α-tocopherol, γ-oryzanol and phytosterol in rice bran oil*, Food Chemistry, 128431, 2021.
[5]. Jeyaprakash D., Dinh D. N., Sutha S., Ganesh D. S., Sundaram A., Atabani A. E., Soon W. C., Gopalakrishnan K., *Engine performance, emission and bio characteristics of rice bran oil derived biodiesel blends*, Fuel, 239, p. 153-161, 2019.
[6]. Novy S. K., Hong C., Yi-Hsu J., *Recovery of gamma-oryzanol from biodiesel residue. Engineers*, Vol. 38, issues 3-4, p. 229-234, 2007.
[7]. Shailendra S., Avinash K. A., Sanjeev G., *Biodiesel development from rice bran oil: Transesterification process*

optimization and fuel characterization, Energy Conversion and Management 49, p. 1248-1257, 2008.
[8]. Shiu P. J., Gunawan S., Hsieh W. H., Kasim N. S., Yi-Hsu J., *Biodiesel production from rice bran by a two-step in-situ process*, Bioresource Technology, 101, p. 984-989, 2010.
[9]. Mayank C., Ajay S., Gaurav D., *Performance evaluation of diesel engine using rice bran biodiesel*, Egyptian Journal of Petroleum, 26, p. 511-518, 2017.
[10]. Lin L., Ying D., Chaitep S., Vittayapadung S., *Biodiesel production from crude rice bran oil and properties as fuel*, Applied Energy, 86, p. 681-688, 2009.
[11]. Srilatha K., Sree R., Prabhavathi Devi B. L. A., Sai Prasad P. S., Prasad R. B. N., Lingaiah N., *Preparation of biodiesel from rice bran fatty acids catalyzed by heterogeneous cesium-exchanged 12-tungstophosphoric acids*, Bioresource Technology, 116, p. 53-57, 2012.
[12]. Zhengqiang X., Fan F., Xiaodong L., Yanning L., *Preparation of an environmentally friendly emulsion-type lubricant based on crude rice bran wax*, Petroleum, 5, p. 77-84, 2019.
[13]. Rajaganapathy C., Rajamurugan T. V., Dyson B. A., Murugapoopathi S., Armstrong M., *A study on tribological behavior of rice bran and karanja oil-based TiO_2 nano bio-fluids*, Materials Today: Proceedings, 2022.
[14]. Rubalya V. S., Arockia J. K., Phebee A. D. R., Uma S., Ashvanth B., *Synthesis and characterisation of electro-rheological property of novel eco-friendly rice bran oil and nanofluid*, Journal of Molecular Liquids, 256, p. 256-266, 2018.
[15]. Albino A. S, Lanza M., Hense H., *Rheological properties of rice bran (Oryza sativa L.) oils processing and soapstock distillation residue*, Industrial Crops and Products, 46, p. 111-116, 2013.
[16]. Rani S., Joy M. L., Prabhakaran N. K., *Evaluation of physiochemical and tribological properties of rice bran oil – biodegradable and potential base stoke for industrial lubricants*, Industrial Crops and Products, 65, p. 328-333, 2015.
[17]. Panchal T. M., Patel A., Chauhan D. D., Thomas M., Jigar V. Patel J. V., *A methodological review on bio-lubricants from vegetable oil-based resources*, Renewable and Sustainable Energy Reviews, 70, p. 65-70, 2017.
[18]. Zainal N. A., Zulkifli N. W. M., Gulzar M., Masjuki H. H., *A review on the chemistry, production, and technological potential of biobased lubricants*, Renewable and Sustainable Energy Reviews, 82, p. 80-102, 2018.
[19]. Krishna C., Ankit K., Venkatasubramaniam L., Ammar H. E., Mohamed K. A. A., *A review of the tribological and thermophysical mechanisms of bio-lubricants based nanomaterials in automotive applications*, Journal of Molecular Liquids, 339, 116717, 2021.
[20]. Oliveira R., Oliveira V., Aracava K. K., Rodrigues C. E. C., *Effects of the extraction conditions on the yield and composition of rice bran oil extracted with ethanol - A response surface approach*, Food and Bioproducts Processing, 90, p. 22-31, 2012.
[21]. Capellini M. C., Giacomini V., Cuevas M. S., Rodrigues C. E. C., *Rice bran oil extraction using alcoholic solvents: Physicochemical characterization of oil and protein fraction functionality*, Ind. Crops Prod. 104, p. 133-143, 2017.
[22]. Imsanguan P., Roaysubtawee A., Borirak R., Pongamphai S., Douglas, S., Douglas P., *Extraction of α- Tocopherol and γ-Oryzanol from Rice Bran*, LWT - Food Sci. Technol. 41, p. 1417-1424, 2008.
[23]. Sneh P., Manoj K., Anil K. S., Sukhvinder S. P., *Rice Bran Oil: Emerging Trends in Extraction, Health Benefit, and Its Industrial Application*, Rice Science, 28(3), p. 217-232, 2021.
[24]. ***, *CIE Technical Report., Colorimetry*, 3rd ed., Publication 15, Central Bureau of the CIE, Vienna, 2004.
[25]. Florea T., *Chimia Alimentelor*, Ed. Academica, p. 353, 2008.

THE ANNALS OF "DUNAREA DE JOS" UNIVERSITY OF GALATI
FASCICLE IX. METALLURGY AND MATERIALS SCIENCE
N°. 3 - 2022, ISSN 2668-4748; e-ISSN 2668-4756
Article DOI: https://doi.org/10.35219/mms.2022.3.02

VITRIFICATION OF IRON OXIDE RICH SLUDGE RESULTED FROM THE GROUNDWATER TREATMENT AS NEW GLASS CERAMIC MATERIALS

Cosmin VANCEA, Giannin MOSOARCA, Simona POPA, Sorina BORAN
Politehnica University Timisoara, Faculty of Industrial Chemistry and Environmental Engineering, Romania
e-mail: cosmin.vancea@upt.ro

ABSTRACT

This paper offers a new solution to vitrify the sludge resulted from washing the filters used for iron removal phase of the groundwater treatment process. The new glass ceramic materials, obtained after heat treatment at three different temperatures: 800, 900 and 1000 °C were characterized in terms of dimensional stability after firing, apparent density and porosity, hydrolytic stability and iron ions immobilization capacity. The effect of the calcined sludge amount upon the mentioned properties was analysed.

KEYWORDS: glass wastes, sludge waste, vitrification, glass ceramics

1. Introduction

The actual increase of industrial and agriculture wastes amounts primarily require an effective management of solid waste worldwide and is a major environmental concern. Due to insufficient space for land-filling and increasing cost for land disposal, it has become essential to recycle and reutilize these industrial waste [1]. Waste recycling provides alternative materials that facilitate the reduction in the depletion rate of natural materials [2] and also the space for land-filling [3].

Glass recycling become a very attractive concept in the last decades because it has been committed to developing technologies to comply with environmental policies [4]. In this context, it is necessary to create new recycling glass strategies because it is not biodegradable and remains stable for a long time [5]. The recycling of glass brings numerous benefits: reduction in raw material extraction [6], energy savings [6, 7], quality conservation [8], waste reduction [9] and decrease of the environmental contaminant [10].

The glass wastes vitrification is an energy consuming process that is economically viable only by manufacturing new glass-based products, such as glazes [11] glass ceramics [12], glass or glass-ceramic matrix composites [13, 14], glass fibres [15] glass foams [16, 17], and others. A new direction for glass wastes recycling is the vitrification of potential hazardous materials: municipal wastes [18-20], hospital wastes [21], radioactive wastes [22] etc.

The current work aims to offer a new alternative to use the sludge resulting from washing the filters used for iron removal in the groundwater treatment by vitrification together with packaging glass waste and kaolin as vitreous ceramic products able to retain iron ions in the glass-ceramic matrix.

2. Materials and methods

The bottle glass waste used have the oxide composition, determined using an RX fluorescence analyser type Niton XL 3, is presented in the Table 1.

The glass waste was grinded in a Pulverisette type laboratory mill using the material-balls-water ratio of 1:2:1, dried in an oven at 105 °C for 24 hours and then sieved, the granulometric fraction corresponding to passing through the 100 µm mesh sieve being retained.

The oxide composition of the used Bojidar kaolin, provided by the SC IPEC SA supplier is presented in the Table 2.

The sludge used comes from the process of washing the filters used for iron removal in the filtration process stage I for groundwater treatment plant SC Aquatim SA. It was dried and calcined at 750 °C for 6 hours. The main ions present in its composition, determined using RX fluorescence analyser type Niton XL 3, are indicate in the Table 3.

The glass ceramic samples were prepared based on the three mentioned precursors using the recipes detailed in the Table 4.

THE ANNALS OF "DUNAREA DE JOS" UNIVERSITY OF GALATI
FASCICLE IX. METALLURGY AND MATERIALS SCIENCE
Nº. 3 - 2022, ISSN 2668-4748; e-ISSN 2668-4756
Article DOI: https://doi.org/10.35219/mms.2022.3.02

Table 1. *The oxide composition of used glass waste*

Oxide	SiO_2	Na_2O	K_2O	CaO	MgO	Al_2O_3	Fe_2O_3
Amount (%)	74.42	12.90	0.19	11.27	0.46	0.75	0.01

Table 2. *The composition of Bojidar kaolin*

Oxide	SiO_2	Na_2O	K_2O	CaO	MgO	Al_2O_3	Fe_2O_3	TiO_2	P.C.
Amount (%)	49.29	0.14	0.87	0.56	0.44	35.18	0.78	0.43	12.31

Table 3. *The composition from the iron removal sludge*

Ion	Fe^{3+}	Mn^{2+}	Ca^{2+}
Amount (%)	83.00	10.03	5.41

Table 4. *Recipes for glass ceramic preparation*

Sample	Precursor amount (%)		
	Glass waste	Calcined sludge	Kaolin
1	60	0	40
2	50	10	40
3	40	20	40
4	30	30	40

The firing treatment was carried out in an electric furnace for 60 minutes at 800, 900 and 1000 ºC respectively.

The samples dimensional deviations after firing were measured using an electronic calliper as the average value of three independent replicates.

The apparent density of the obtained foam glasses was measured using the liquid saturation method under vacuum with water as a working liquid.

The hydrolytic stability of the samples was determined according to ISO 719-1985. Two grams of grinded samples, having particles size less than 500 μm, were kept for 60 min in 50 mL deionized water at 98 °C. The volume of HCl needed for neutralization is recorded in order to express the equivalent Na_2O extracted.

The iron immobilization capacity was investigated by measuring the Fe^{3+} ions extraction using leaching tests performed according to the American Extraction Procedure Toxicity Test [23]. Deionized water was used as extraction medium at a constant temperature of 20 ± 2 °C, analysis being performed after 28 days using a Bruker Aurora ICP-MS.

3. Results and Discussion

3.1. Dimensional deviations after the firing process

The glass ceramic shrinkage after the heat treatment is due to the structural changes that occur at high temperature. The volume contractions of the samples during combustion are shown Figure 1 for the three firing temperatures used for synthesis. The lowest shrinkage was recorded for the samples obtained at 800 ºC, ranging between 1.21-1.46 % while the synthesis at 1000 ºC leads to higher dimensional deviations, ranged between 12.31-19.83 %. As the firing temperature increases, the vitreous phase melts and becomes more fluid, occupying the pores in the glass ceramic mass, thus generating a higher shrinkage of the samples. The substitution of the glass waste with calcined sludge leads to a decrease in contractions during firing, less important at a temperature of 800 ºC but more pronounced at 1000 ºC.

3.2. Apparent densities and apparent porosities of the glass ceramics

The apparent density and the apparent porosity of the investigated glass ceramic compositions are illustrated in Figures 2 and 3. The apparent density values range between 1.35-1.71 g/cm^3 for the samples treated at 800 ºC and 1.63-1.88 g/cm^3 for those fired at 1000 ºC. The apparent porosities for the glass ceramics sintered at 800 ºC are between 35.09-56.78 % and between 25.61-43.33% when heat treated at 1000 ºC.

For all the studied samples, increasing the sintering temperature generates larger amount of melted glass that fills the pores, leading to a higher apparent density and a smaller apparent porosity. Replacing the vitreous precursor with calcined sludge waste produces a lower amount of melt able to fill the pores and therefore higher apparent porosities and lower apparent densities were recorded for the three used thermal treatment temperatures.

THE ANNALS OF "DUNAREA DE JOS" UNIVERSITY OF GALATI
FASCICLE IX. METALLURGY AND MATERIALS SCIENCE
No. 3 - 2022, ISSN 2668-4748; e-ISSN 2668-4756
Article DOI: https://doi.org/10.35219/mms.2022.3.02

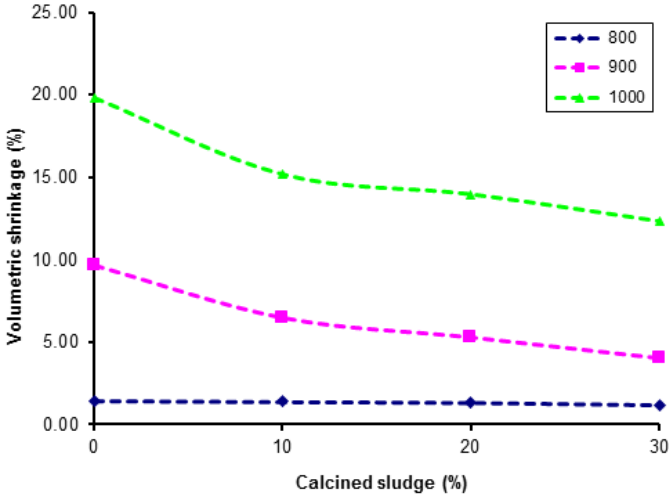

Fig. 1. *Evolution of volume contractions with calcined sludge amount for the studied samples*

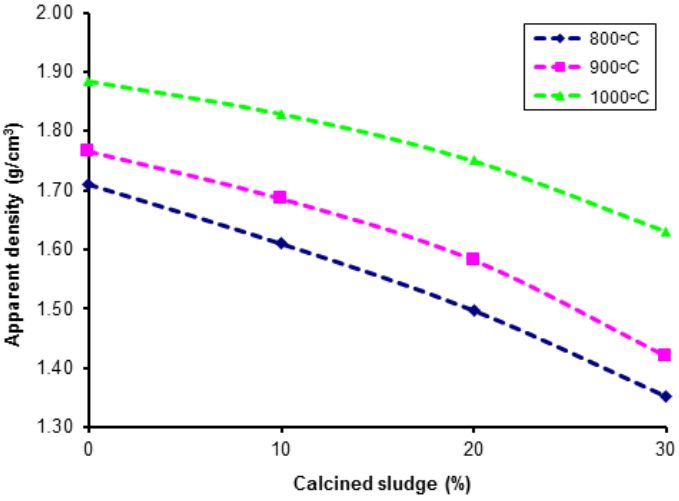

Fig. 2. *Evolution of apparent density with calcined sludge amount for the studied samples*

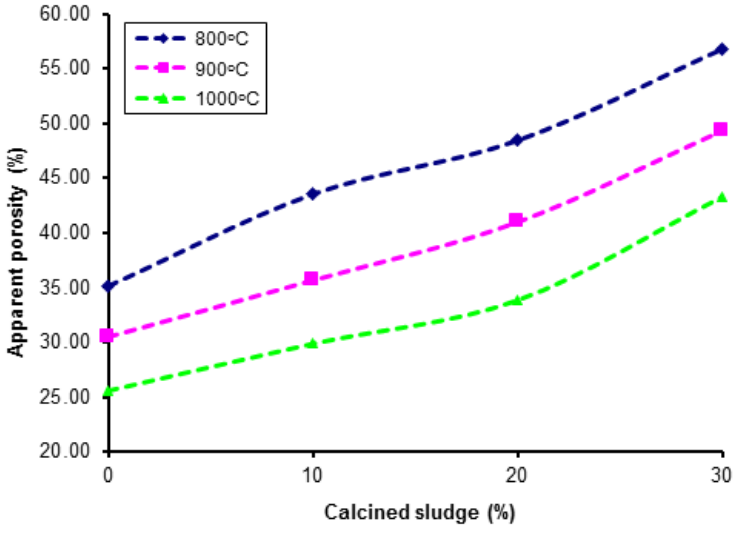

Fig. 3. *Evolution of apparent porosity with calcined sludge amount for the studied samples*

THE ANNALS OF "DUNAREA DE JOS" UNIVERSITY OF GALATI
FASCICLE IX. METALLURGY AND MATERIALS SCIENCE
Nº. 3 - 2022, ISSN 2668-4748; e-ISSN 2668-4756
Article DOI: https://doi.org/10.35219/mms.2022.3.02

3.3. Hydrolytic stability of the studied glass ceramics

The synthesized glass ceramics stability in water was studied according to ISO 719-1985, the obtained results being summarized in Table 5.

Table 5. *Hydrolytic stability class of the investigated glass ceramics*

Firing temp. (ºC)	Calcined sludge (%)	Equivalent Na_2O extracted (mg)	Stability class
800	0	68.75	HGB3
	10	63.5	HGB3
	20	58.15	HGB2
	30	53.25	HGB2
900	0	65.5	HGB3
	10	56.05	HGB2
	20	50.7	HGB2
	30	48.45	HGB2
1000	0	63.25	HGB3
	10	52.5	HGB2
	20	45.2	HGB2
	30	31.75	HGB2

The alkaline oxide is mainly extracted from the vitreous phase; therefore, the glass ceramics hydrolytic stability increases with the increase of the calcined sludge amount. The higher firing temperature leads to a better integration of the vitreous phase in the glass ceramic matrix, being less exposed toward the water dissolution.

3.4. Iron ions immobilization in the glass ceramics matrix

Iron ions dissolution from the studied glass ceramics after 28 days in deionized water are illustrated in Figure 4.

The amounts of Fe^{3+} extracted after 28 days, for all the samples studied, were extremely low, ranging between 0-0.0023%. The increase in the amount of calcined sludge due to the corresponding decrease in the amount of waste glass leads to an increase of the Fe^{3+} leached, due to the fact that the sludge is the main vector carrying iron ions in the studied masses.

The increase in the firing temperature generates a decrease of iron leached due to an increase of the encapsulation of the calcined sludge waste, associated with a better melting of the glass particles.

This confirms the very good iron immobilization capacity in the studied glass-ceramic matrices.

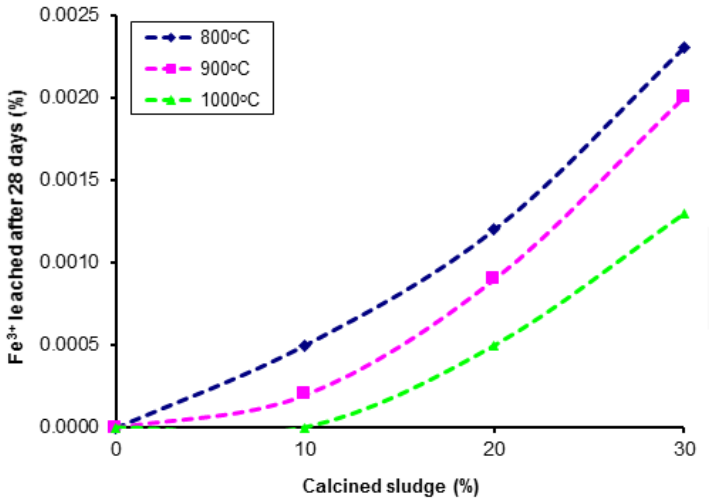

Fig. 4. *Evolution of iron ions leached after 28 days with calcined sludge amount for the studied samples*

4. Conclusions

Glass ceramic masses were synthesized starting from bottle glass wastes and a calcined sludge waste rich in Fe_2O_3 derived from the washing process of the filters used for iron removal in the groundwater treatment together with kaolin as main ceramic precursor.

The dimensional stability of the obtained samples after the firing process range between 1.21-1.46% at 800 ºC and 12.31-19.83% at 1000 ºC respectively. The substitution of the glass waste with calcined sludge leads to an increase of the dimensional stability after the heat treatment.

The apparent density of the synthesized samples range between 1.35-1.88 g/cm^3 while the apparent porosity values are between 25.91-56.78%,

depending of the firing temperature. Using higher amounts of calcined sludge waste generates a lower quantity of melt to fill the pores and leading to higher apparent porosities and lower apparent densities.

The hydrolytic stability of the glass ceramics samples, studied according with ISO 719-1985, qualifies them as HGB2-HGB3 materials, having good water resistance. The samples hydrolytic stability increases with the increase of the calcined sludge amount.

The obtained glass ceramic matrix immobilized iron ions very well, the lixiviation values after 28 days range between 0-0.0023% of the total iron content. The increase in the amount of calcined sludge leads to an increase of the Fe^{3+} leached, the sludge being the main vector carrying iron ions in the investigated materials.

These results confirm the viability of the proposed solution for immobilizing iron rich calcined sludge in glass ceramic matrix using bottle glass wastes and kaolin as precursor materials, with multiple economic advantages.

References

[1]. Samadi M., Huseien G. F., Mohammadhosseini H., Lee H. S., Abdul Shukor Lim N. H., Md Tahir M., Alyousef R., *Waste ceramic as low cost and eco-friendly materials in the production of sustainable mortars*, Journal of Cleaner Production, 266, 121825, 2020.

[2]. Ogundairo T. O., Adegoke D. D., Akinwumi I. I., Olofinnade O. M., *Sustainable use of recycled waste glass as an alternative material for building construction – A review*, IOP Conf. Series: Materials Science and Engineering, 640, 012073, 2019.

[3]. García Guerrero J., Rodríguez Reséndiz J., Rodríguez Reséndiz H., Álvarez-Alvarado J. M., Rodríguez Abreo O., *Sustainable Glass Recycling Culture-Based on Semi-Automatic Glass Bottle Cutter Prototype*, Sustainability 13, 6405, 2021.

[4]. Kuo-Yi L., *User experience-based product design for smart production to empower industry 4.0 in the glass recycling circular economy*, Computers & Industrial Engineering, 125, p. 729-738, 2018.

[5]. Ibrahim S., Meawad A., *Assessment of waste packaging glass bottles as supplementary cementitious materials*, Construction and Building Materials, 182, p. 451-458, 2018.

[6]. Larsen A. W., Merrild H., Christensen T. H., *Recycling of glass: accounting of greenhouse gases and global warming contributions*, Waste Management & Research, 27(8), p. 754-762, 2009.

[7]. Testa M., Malandrino O., Sessa M. R., Supino S., Sica D., *Long-term sustainability from the perspective of cullet recycling in the container glass industry: Evidence from Italy*, Sustainability, 9(10), 1752, 2017.

[8]. Sudharsan N., Palanisamy T., Yaragal S. C., *Environmental sustainability of waste glass as a valuable construction material-A critical review*, Ecology, Environment and Conservation, 24, p. S331-S338, 2018.

[9]. Hamzah K. H., Huseien G. F., Asaad M. A., Georgescu D. P., Ghoshal S. K., Alrshoudi F., *Effect of waste glass bottles-derived nanopowder as slag replacement on mortars with alkali activation: Durability characteristics*, Case Studies in Construction Materials, 15, e00775, 2021.

[10]. Sarkis C. J. L., Raich O. M., Mestre J. L. Z., *Assessment of the temperature of waterproofing membrane when a recycled crushed glass finish layer is used on flat roofs to protect from sun radiance*, Energy Procedia, 115, p. 451-462, 2017.

[11]. Gol F., Yilmaz A., Kacar E., Simsek S., Sarıtas Z. G., Ture C., Arslan M., Bekmezci M., Burhan H., Sen F., *Reuse of glass waste in the manufacture of ceramic tableware glazes*, Ceramics International, 47, 15, 2021.

[12]. Silva R. V., de Brito J., Lye C. Q., Dhir R. K., *The role of glass waste in the production of ceramic-based products and other applications: A review*, Journal of Cleaner Production, 167, p. 346-364, 2017.

[13]. Paknahad E., Grosvenor A. P., *Investigation of the stability of glass-ceramic composites containing* $CeTi_2O_6$ *and* $CaZrTi_2O_7$ *after ion implantation*, Solid State Sciences, 74, p. 109-117, 2017.

[14]. Luhar S., Cheng T. W., Nicolaides D., Luhar I., Panias D., Sakkas K., *Valorisation of glass wastes for the development of geopolymer composites – Durability, thermal and microstructural properties: A review*, Construction and Building Materials, 222, p. 673-687, 2019.

[15]. Karuppannan Gopalraj S., Kärki T., *A review on the recycling of waste carbon fibre/glass fibre-reinforced composites: fibre recovery, properties and life-cycle analysis*, SN Applied Sciences, 2, 433, 2020.

[16]. Stochero N. P., de Souza Chami J. O. R., Souza M. T., de Moraes E. G., Novaes de Oliveira A. P., *Green Glass Foams from Wastes Designed for Thermal Insulation*, Waste and Biomass Valorization, 12, p. 1609-1620, 2021.

[17]. Taurino R., Lancellotti I., Barbieri L., Leonelli C., *Glass-Ceramic Foams from Borosilicate Glass Waste*, International Journal of Applied Glass Science, 5, p. 136-145, 2014.

[18]. Stabile P., Bello M., Petrelli M., Paris E., Carroll M. R., *Vitrification treatment of municipal solid waste bottom ash*, Waste Management, 95, p. 250-258, 2019.

[19]. Pei S. L., Chen T. L., Pan S. Y., Yang Y. L., Sun Z. H., Li Y. J., *Addressing environmental sustainability of plasma vitrification technology for stabilization of municipal solid waste incineration fly ash*, Journal of Hazardous Materials, 398, 122959, 2020.

[20]. Sharifikolouei E., Baino F., Salvo M., Tommasi T., Pirone R., Fino D., Ferraris M., *Vitrification of municipal solid waste incineration fly ash: An approach to find the successful batch compositions*, Ceramics International, 47, p. 7738-7744, 2021.

[21]. Stoch P., Ciecińska M., Stoch A., Kuterasiński Ł., Krakowiak I., *Immobilization of hospital waste incineration ashes in glass-ceramic composites*, Ceramics International, 44, p. 728-734, 2018.

[22]. Zhang Y., Kong L., Ionescu M., Gregg D. J., *Current advances on titanate glass-ceramic composite materials as waste forms for actinide immobilization: A technical review*, Journal of the European Ceramic Society, 42, p. 1852-1876, 2022.

[23]. ***, *Extraction procedure toxicity test in: Stabilization/Solidification of CERCLA and RCRA Wastes*, US EPA625/6-89/022, US EPA, Cincinnati, Ohio, 1986.

THE ANNALS OF "DUNAREA DE JOS" UNIVERSITY OF GALATI
FASCICLE IX. METALLURGY AND MATERIALS SCIENCE
Nº. 3 - 2022, ISSN 2668-4748; e-ISSN 2668-4756
Article DOI: https://doi.org/10.35219/mms.2022.3.03

GREEN SYNTHESIS OF METAL NANOPARTICLES USING MICROALGAE: A REVIEW

Rodica CHIHAI (PEȚU), Alina-Florentina SĂRACU, Claudia-Veronica UNGUREANU
"Dunarea de Jos" University of Galati, Cross-Border Faculty, Romania
e-mail: claudia.ungureanu@ugal.ro

ABSTRACT

Nanometallic materials are metals and alloys that form nanocrystalline grains with particle size of about 5 to100 nm. In materials science, "green synthesis" has become a reliable, sustainable, and eco-friendly protocol for synthesizing a wide range of materials such as metal oxides, hybrids, and bio-inspired materials. Nowadays, a wide range of physico-chemical methods are used for the synthesis of nanoparticles. Green synthesis is found to be superior over physical and chemical method as it is economically feasible, environmentally friendly, scaled up for mass-scale production without any complexity. Several biological approaches, including the utilization of plant extracts, enzymes, bacteria, fungi, and algae, are being studied in order to enable a more environmentally sound synthesis of nanoparticles. Because these techniques are regarded as safe and environmentally responsible for the production of nanomaterials as an alternative to conventional methods, the development of green methods for the synthesis of nanoparticles is developing into a significant area of nanotechnology.

KEYWORDS: microalgae, silver nanoparticles, eco-friendly

1. Background

In order to lessen the negative impacts of nanoparticles frequently utilized in laboratories and industry by conventional synthesis methods, green synthesis is seen as a crucial instrument [1].

Over the last decade, the field of processing algal biomass under catalytic conditions has received a lot of interest. Algae could be considered as a "bio-factory" for synthesis of metallic nanoparticles. Also, algae are well known for their ability to hyper-accumulate heavy metal ions and remodel into more malleable shapes [2].

Algae are a group of autotropic organisms with economic and ecological importance. They are single or multicellular organisms that live in different habitats, such as freshwater, marine water, or damp rock surfaces. The two different categories of algae are microalgae (microscopic) and macroalgae (macroscopic). They play a vital role in applications such as medicine, pharmacy, forestry, aquaculture, and cosmetics. They are an important source of several commercial products including natural dyes and biofuel [3].

Algae have so been suggested as a model organism for producing bio-nanomaterials. Physical variables like pH, reaction time, exposure time, precursor concentration and temperature affect how nanoparticles form, grow, and stabilize. To alter the size and morphology of the cells and prevent aggregation, these factors can be changed. According to the species and age of the algae, phycocyanin and phycoerythrin contain varying concentrations of carbohydrates, proteins, minerals, vitamins, fatty acids, antioxidants, and pigments. Theoretically, these active substances have been referred to as reducing and stabilizing agents in the creation of nanoparticles [2, 4].

Due to their capacity to reduce metal ions, nanoparticles made from a variety of different algal resources have emerged as one of the most cutting-edge and current areas of biochemical research [5]. Depending on the algae species and method of activity, nanoparticles can be synthesized intracellularly or extracellularly [6].

In comparison to bigger particles, nanoparticles are gaining recognition as complex materials with innovative or cutting-edge properties. Pharmaceutical, industrial, and biotechnological uses all rely heavily

THE ANNALS OF "DUNAREA DE JOS" UNIVERSITY OF GALATI
FASCICLE IX. METALLURGY AND MATERIALS SCIENCE
Nº. 3 - 2022, ISSN 2668-4748; e-ISSN 2668-4756
Article DOI: https://doi.org/10.35219/mms.2022.3.03

on nanoparticles. Due to its distinctive qualities in the fields of technology, science, and medical, such as antimicrobial, catheters, food containers, and anticancer, silver nanoparticles have drawn the attention of researchers in recent years [7].

The synthesis of nanoparticles must be done using methods that follow a "green" path because nanoparticles are used in consumer health and industrial products. Several biological approaches, including the utilization of plant extracts, enzymes, bacteria, fungi, and algae, are being studied in order to enable a more environmentally sound synthesis of nanoparticles [8].

This review gives an insight of various updated reports of synthesis of advance nanomaterials using green and simple approach rather than using complicated procedures, hazardous, toxic chemicals for the synthesis of nanomaterials.

2. Biosynthesis of Silver Nanoparticles by Microalgae

In light of the wide applications of AgNPs, their synthesis becomes a very crucial factor. Three different approaches can be used for the synthesis of nanoparticles, namely physical, chemical, and biological or green synthesis.

Recent developments show the critical role of microorganisms and biological systems in production of metal nanoparticles. The use of organisms in this area is rapidly developing due to their growing success and ease of formation of nanoparticles. Moreover, biosynthesis of metal nanoparticles is an environmentally friendly method (green chemistry) without use of harsh, toxic and expensive chemicals. [9].

To cultivate diverse algae species, the researchers employed a variety of techniques, including open culture systems (such as open ponds, tanks, and raceway ponds) and closed cultivation systems (such as photo bioreactors) [10].

In the bulk of the investigations, the following key processes for the production of metal nanoparticles utilizing algae are seen:

- Boiling or heating an algal extract for a predetermined amount of time in water or an organic solution.
- Making molar solutions of ionic metallic compounds.
- Under carefully monitored conditions, both algae and solutions of ionic metallic compounds are incubated for a predetermined amount of time, either with frequent stirring or without [11].

In addition to being widely employed in hard surface products and textiles, silver and silver nanoparticles are also used in a wide range of pharmaceutical, food industrial, and domestic applications.

Usually, an algal species synthesized NP by accumulating and subsequently reducing the cations. They can be synthesized from algal biomass using either the extracellular or intracellular mechanism.

The bio-reduction of a metal ion to its nanoparticle occurs on the surface of the algal cell in the extracellular pathway whereas in the intra-cellular mechanism the bio-reduction through enzymatic activity occurs inside the cell wall and cell membrane [12]. However, most studies related to the synthesis of silver nanoparticles with the algal biomass involve.

Silver nanoparticles were used in *Chlorella vulgaris* conditioned media, which changed colour from bright yellow to dark brown (UV-VIS absorbance at 415 nm) [13, 14].

Chokshi and collaborators, have reported using degreased algal biomass (*Acutodesmus dimorphus*) to create silver nanomaterial [15]. Also, three different genera of microalga live cultures: *Nannochloropsis oculata*, *Dunaliella salina*, and *Chlorella vulgaris*, were subjected to three different doses of aqueous $AgNO_3$ solution (1 mM, 2 mM, and 5 mM). It was observed that just two of the three species of algae, *Nannochloropsis oculata* and *Chlorella vulgaris*, were able to produce nanoparticles, and even then, only at a concentration of 1mM $AgNO_3$ [16, 17].

The synthesis of silver nanoparticles using the freshwater cyanobacterium, *Plectonema boryanum* (UTEX 485) has been already reported [18].

Spirulina in food causes unique therapeutic effects including immunomodulation, anticancer, antioxidant antiviral and antibacterial, metalloprotective [19, 20]. *Arthrospira platensis* is the most available and commonly utilized genus and has been the subject of many studies in the food and pharmaceutical industries [21, 22]. Also, can rapidly produce Ag nanoparticles through extracellular biosynthesis.

Once the NPs are synthesized, their conformational details about shape, size, dispersity, homogeneity as well as surface morphology are determined by using various techniques, including: energy dispersive X-ray spectroscopy (EDX), scanning electron microscopy (SEM), UV-VIS absorption spectroscopy, transmission electron microscopy (TEM), Fourier transmission infrared (FTIR) spectroscopy and dynamic light scattering (DLS) (Figure 1) [23].

THE ANNALS OF "DUNAREA DE JOS" UNIVERSITY OF GALATI
FASCICLE IX. METALLURGY AND MATERIALS SCIENCE
Nº. 3 - 2022, ISSN 2668-4748; e-ISSN 2668-4756
Article DOI: https://doi.org/10.35219/mms.2022.3.03

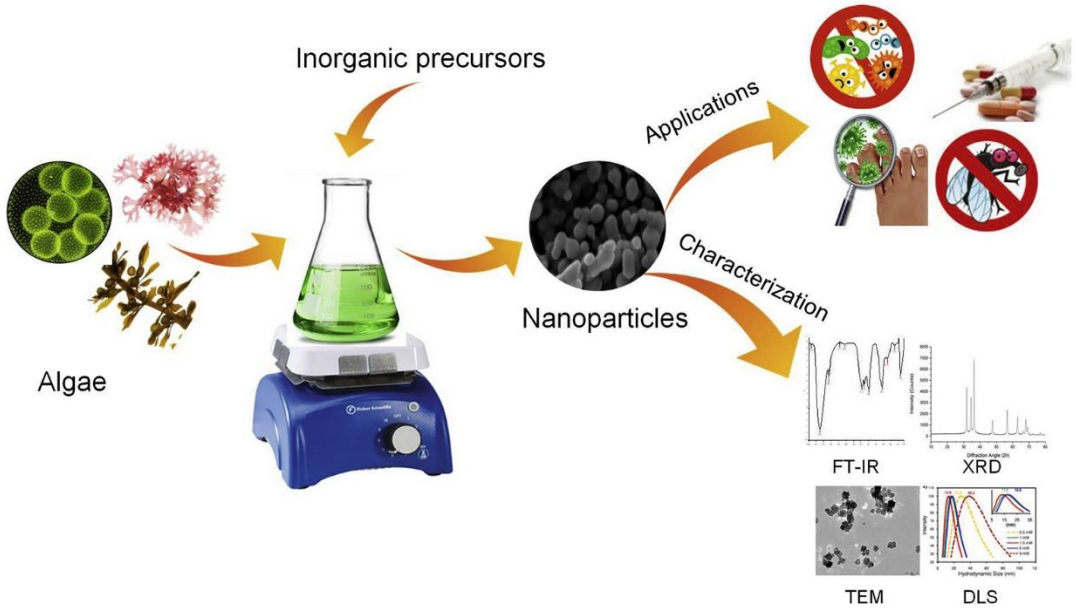

Fig. 1. *Synthesis of silver nanoparticles*

Researchers mostly utilize analytical techniques such as TEM and SEM for morphological analysis of silver nanoparticles. For studies, the sample are sputter-coated on copper grids with a metal nanoparticle solution, dried, and then ready for analysis. Additionally, for improved identification, SEM and TEM are combined with an energy dispersive X-ray analysis (EDX). Is another tool that gives information about symmetry, size and phase identification of metallic nanoparticles [24]. Also, UV-VIS spectra are used to examine the size and shape of metallic nanoparticles in aqueous solution and FTIR spectroscopy is employed to determine the nature of functional groups of active components on the surface of nanoparticles.

Because of their special qualities including catalytic activity and stability, silver NPs are regarded as excellent. Additionally, they have anti-bacterial, anti-viral, and anti-fungal effects. AgNPs are used in antibacterial nanodevices as one of its applications due of their Ag^{+} ion action. They have an anti-proliferative impact and can cause cell death, making them effective anti-cancer drugs [25, 26].

AgNPs may be loaded or coated to lessen their toxicity and extend their biological retention period, enabling the targeted killing of malignant cells. AgNPs from *Andrographis echioides* are frequently employed in human breast cancer cell lines and have been proven to impede the development of MCF-2 cells [27, 28]. The viability of tumour cells decreases when the concentration of AgNPs rises. gastrointestinal cancer has responded favourably to *Allium sativum* AgNPs [29, 30].

3. Conclusions

Nanotechnology is improving our everyday lives by enhancing the performance and efficiency of everyday objects. It provides a clean environment by providing safer air and water, and clean renewable energy for a sustainable future. Due to their incredible properties, metallic nanoparticles have been widely used for many applications such as energy, health science, environment, agriculture field etc.

Use of microalgae for the synthesis of nanoparticles could be considered as an eco-friendly approach due to less time consuming, inexpensive, environmental compatibility, scalability, and nanoparticle stabilization compared to the chemical synthesis procedures. However, the use of microalgae for nanoparticle synthesis have not been extensively researched.

In addition, nano-biotechnology that uses algae and microalgae to synthesize nanomaterials is still in its early stages, and further research and development is required.

Acknowledgements

This work was supported by an intern grant "Microbiological synthesis of metal nanoparticles", project number 14889/11.05.2022.

References

[1]. Singh R., Upadhyay A. K., Chandra P., Singh D. P., *Sodium chloride incites reactive oxygen species in green algae* Chlorococcum humicola *and* Chlorella vulgaris*: implication on*

THE ANNALS OF "DUNAREA DE JOS" UNIVERSITY OF GALATI
FASCICLE IX. METALLURGY AND MATERIALS SCIENCE
Nº. 3 - 2022, ISSN 2668-4748; e-ISSN 2668-4756
Article DOI: https://doi.org/10.35219/mms.2022.3.03

lipid synthesis, mineral nutrients and antioxidant system, Bioresource technology, 270, p. 489-497, 2018.

[2]. Fawcett D., Verduin J. J., Shah M., Sharma S. B., Poinern G. E. J., *A review of current research into the biogenic synthesis of metal and metal oxide nanoparticles via marine algae and seagrasses*, Journal of Nanoscience, 2017.

[3]. Lewis Oscar F., Vismaya S., Arunkumar M., Thajuddin N., Dhanasekaran D., Nithya C., *Algal Nanoparticles: Synthesis and Biotechnological Potentials*, Algae - Organisms for Imminent Biotechnology, p. 157-182, 2016.

[4]. Mukherjee A., Sarkar D., Sasmal S., *A review of green synthesis of metal nanoparticles using algae*, Frontiers in Microbiology, 12, 2021.

[5]. Ponnuchamy K., Jacob J. A., *Metal nanoparticles from marine seaweeds – a review*, Nanotechnology Reviews, 5(6), p. 589-600, 2016.

[6]. Chaudhary R., Nawaz K., Khan A. K., Hano C., Abbasi B. H., Anjum S., *An overview of the algae-mediated biosynthesis of nanoparticles and their biomedical applications*, Biomolecules, 10(11), 1498, 2020.

[7]. Mustapha T., Misni N., Ithnin N. R., Daskum A. M., Unyah N. Z., *A Review on Plants and Microorganisms Mediated Synthesis of Silver Nanoparticles, Role of Plants Metabolites and Applications*, International Journal of Environmental Research and Public Health, 19(2), 674, 2022.

[8]. Ahmed S., Ahmad M., Swami B. L., Ikram S., *A review on plants extract mediated synthesis of silver nanoparticles for antimicrobial applications: a green expertise*, Journal of advanced research, 7(1), p. 17-28, 2016.

[9]. Bahrulolum H., Nooraei S., Javanshir N., Tarrahimofrad H., Mirbagheri V. S., Easton A. J., Ahmadian G., *Green synthesis of metal nanoparticles using microorganisms and their application in the agrifood sector*, Journal of Nanobiotechnology, 19(1), p. 1-26, 2021.

[10]. Narala R. R., Garg S., Sharma K. K., Thomas-Hall S. R., Deme M., Li Y., Schenk P. M., *Comparison of microalgae cultivation in photobioreactor, open raceway pond, and a two-stage hybrid system*, Frontiers in Energy Research, 4, 29, 2016.

[11]. Uzair B., Liaqat A., Iqbal H., Menaa B., Razzaq A., Thiripuranathar G., Menaa F., *Green and cost-effective synthesis of metallic nanoparticles by algae: Safe methods for translational medicine*, Bioengineering, 7(4), 129, 2020.

[12]. Almatroudi A., *Silver nanoparticles: Synthesis, characterisation and biomedical applications*, Open life sciences, 15(1), p. 819-839, 2020.

[13]. Chokshi K., Pancha I., Ghosh T., Paliwal C., Maurya R., Ghosh A., Mishra S., *Green synthesis, characterization and antioxidant potential of silver nanoparticles biosynthesized from de-oiled biomass of thermotolerant oleaginous microalgae* Acutodesmus dimorphus, RSC advances, 6(76), p. 72269-72274, 2016.

[14]. Da Silva Ferreira V., Conz Ferreira M. E., Lima L. M. T., Frasés S., de Souza W., Sant'Anna C., *Green production of microalgae-based silver chloride nanoparticles with antimicrobial activity against pathogenic bacteria*, Enzyme and Microbial Technology, 97, p. 114-121, 2017.

[15]. Mukherjee A., Sarkar D., Sasmal S., *A review of green synthesis of metal nanoparticles using algae*, Frontiers in Microbiology, 12, 2021.

[16]. Mohseniazar M., Barin M., Zarredar H., Alizadeh S., Shanehbandi D., *Potential of microalgae and lactobacilli in biosynthesis of silver nanoparticles*, BioImpacts: BI, 1(3), 149, 2011.

[17]. Chugh D., Viswamalya V. S., Das B., *Green synthesis of silver nanoparticles with algae and the importance of capping agents in the process*, Journal of Genetic Engineering and Biotechnology, 19(1), p. 1-21, 2021.

[18]. Mubarak Ali D., Arunkumar J., Nag K. H., Sheik Syed Ishack K. A., Baldev E., Pandiaraj D., Thajuddin N., *Gold nanoparticles from Pro and eukaryotic photosynthetic microorganisms - Comparative studies on synthesis and its application on biolabeling*. Colloids and Surfaces B: Biointerfaces, 103, p. 166-173, 2013.

[19]. Marzieh H. S., Shahbazizadeh S., Khosravi-Darani K., Reza M. M., Spirulina paltensis*: Food and function*, Current Nutrition & Food Science, 9, p. 189-193, 2013.

[20]. Zaid A. A., Hammad D. M., Sharaf E. M., *Antioxidant and anticancer activity of Spirulina platensis water extracts*, International Journal of Pharmacology, 11, p. 846-51, 2015.

[21]. Pathak J., Ahmed H., Singh D. K., Pandey A., Singh S. P., Sinha R. P., *Recent developments in green synthesis of metal nanoparticles utilizing cyanobacterial cell factories*, Nanomaterials in Plants, Algae and Microorganisms, p. 237-65, 2019.

[22]. Narayanan K. B., Sakthivel N., *Biological synthesis of metal nanoparticles by microbes*, Advances in colloid and interface science, 156, p. 1-13, 2010.

[23]. Arya A., Chundawat T. S., *Metal nanoparticles from algae: A green approach for the synthesis, characterization and their biological activity*, Nanoscience & Nanotechnology-Asia, 10(3), p. 185-202, 2020.

[24]. Chaudhary R., Nawaz K., Khan A. K., Hano C., Abbasi B. H., Anjum S., *An overview of the algae-mediated biosynthesis of nanoparticles and their biomedical applications*, Biomolecules, 10(11), 1498, 2020.

[25]. Venugopal K., Rather H. A., Rajagopal K., Shanthi M. P., Sheriff K., Illiyas M., Maaza M., *Synthesis of silver nanoparticles (AgNPs) for anticancer activities (MCF 7 breast and A549 lung cell lines) of the crude extract of* Syzygium aromaticum, Journal of Photochemistry and Photobiology B: Biology, 167, p. 282-289, 2017.

[26]. Mur R., Skulberg O. M., Utkilen H., Cyanobacteria in The Environment, 1999.

[27]. Khanna P., Kaur A., Goyal D., *Algae-based metallic nanoparticles: Synthesis, characterization and applications*, Journal of microbiological methods, 163, 105656, 2019.

[28]. Elangovan K., Elumalai D., Anupriya S., Shenbhagaraman R., Kaleena P. K., Murugesan K., *Phyto mediated biogenic synthesis of silver nanoparticles using leaf extract of Andrographis echioides and its bio-efficacy on anticancer and antibacterial activities*, Journal of Photochemistry and Photobiology B: Biology, 151, p. 118-124, 2015.

[29]. Arivazhagan S., Velmurugan B., Bhuvaneswari V., Nagini S., *Effects of aqueous extracts of garlic (*Allium sativum*) and neem (*Azadirachta indica*) leaf on hepatic and blood oxidant-antioxidant status during experimental gastric carcinogenesis*, Journal of Medicinal Food, 7(3), p. 334-339, 2004.

[30]. Dikshit P. K., Kumar J., Das A. K., Sadhu S., Sharma S., Singh S., Kim B. S., *Green synthesis of metallic nanoparticles: Applications and limitations*, Catalysts, 11(8), 902, 2021.

THE ANNALS OF "DUNAREA DE JOS" UNIVERSITY OF GALATI
FASCICLE IX. METALLURGY AND MATERIALS SCIENCE
Nº. 3 - 2022, ISSN 2668-4748; e-ISSN 2668-4756
Article DOI: https://doi.org/10.35219/mms.2022.3.04

IDENTIFICATION OF CROP DISEASES USING DEEP LEARNING ALGORITHM

Florin Bogdan MARIN, Mihai Gabriel MATACHE, Mihaela MARIN, Carmela GURĂU, Gheorghe GURĂU
"Dunarea de Jos" University of Galati, Romania
e-mail: gheorghe.gurau@ugal.ro

ABSTRACT

In this paper we present an algorithm based on deep learning. The program allows the user to select in a graphical interface the type of plant for which it is desired to insert images for disease identification. To train and test models, we used our own data set with a relatively small number of images, and all images were captured in culture, and not in laboratory conditions. The algorithm is based on deep learning approach.

KEYWORDS: plant disease identification, deep learning, computational fluid dynamics

1. Introduction

Plant diseases have by far a hard influence concerning food production in order to reduce or mitigate losses in production, consequently is of paramount importance that crop diseases are surveyed in a good manner to be detected and act accordingly to the current situation in real time. The nowadays recent large scale of use of deep learning algorithms dedicated to image processing applications in the domain of plant disease detection is providing a highly robust option to achieve extremely accurate results [1].

In general, traditional manual visual observation for disease diagnosis methods is inefficient and time-consuming, especially for small and medium-sized farms. With the modern advancement of computer vision and artificial intelligence algorithms, the plant disease detection protocol has become an integral part of crop health monitoring information collection, which substantially improves the efficiency of plant production [2].

Early identification and prevention of plant diseases are the important aspects of crop harvesting as they can effectively reduce any growth disturbances and thus minimize chemicals use. In this regard, the automatic detection of plant diseases using different machine learning (ML) algorithms has become an effective tool for modern agriculture. Various machine learning approaches such as neural network [3] and support vector machine (SVM) [4] have been used for plant and disease classification. However, such complex pre-processing images and method feature extraction step have lower performance and speed in real-time disease detection. Furthermore, one of the main drawbacks of traditional machine learning approaches is that they are not suitable for real-life discovery scenarios with complex non-uniform backgrounds. In this regard, recently, deep learning has made a significant breakthrough in the field of computer vision with various applications [5].

Artificial Vision (AV) together with Artificial Intelligence (AI), have developed techniques and methods for object recognition and classification with significant progress [7-9]. Deep learning algorithms allows trained data models to learn models using data with multiple levels of abstraction, achieving a high rate of precision in many domains such as object recognition and object detection. There are many basic deep learning models such as Deep Feed Forward, where data extracted from training process is propagated in only one direction in the network through several layers of neurons. There are several algorithms such as: Back-Propagation, Convolutional Neural Network, Recurrent Neural Network, including Long Short-Term Memory, Auto-Encoder, Deep Belief Network, and Deep Reinforcement Learning [8-11]. One particular very used category of feed forward network that may be very easy to be trained compared to fully connected networks is the one peculiar architecture named the convolutional neural network (CNN).

THE ANNALS OF "DUNAREA DE JOS" UNIVERSITY OF GALATI
FASCICLE IX. METALLURGY AND MATERIALS SCIENCE
Nº. 3 - 2022, ISSN 2668-4748; e-ISSN 2668-4756
Article DOI: https://doi.org/10.35219/mms.2022.3.04

2. Technique proposed

CNNs are considered by many scholars a highly powerful algorithm for modeling complex processes for image recognition in application where is required a fast data processing in real time. Many approaches are taken into account highly used architectures such as LeNet, AlexNet, VGGNet, GoogleNet, InceptionV3, ResNet, and DenseNet, allowing increase the recognition rate in plant disease identification. Despite the important highly precision provided by deep learning, several challenges are emerging to the real-life scenarios for the aim of recognition and identification of plant diseases. Several issues such as the genetic diversity of crops and diseases is affecting the results in case of real outdoor plant environment application. AlexNET is an object detection model that transforms the object detection task into a regression problem by generating bounding box coordinates and probabilities corresponding to each class.

In this paper we present an algorithm based on deep learning. The program allows the user to select in a graphical interface the type of plant for which it is desired to insert images for disease identification (Fig. 2).

According to our approach, during object detection, the input image is processed successively with 5 convolution and 2 pooling operations. The final layer is a fully connected layer with the confidence scores and conditional probabilities of the corresponding class for each target class (Fig. 1).

The classification problem also considers the position detection task. The purpose of the model is to identify a class of diseases. The algorithm is able to detect 17 classes of disease.

The image might be acquired by any means, using a phone camera, and any digital.

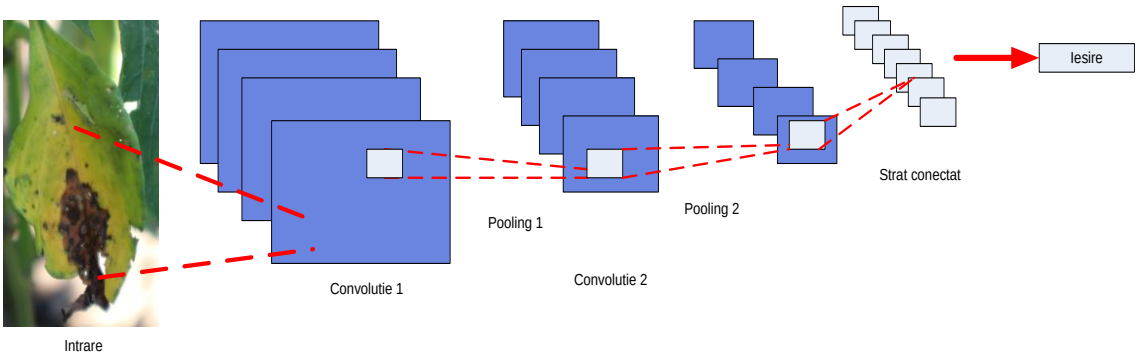

Fig. 1. *Deep learning algorithm architecture*

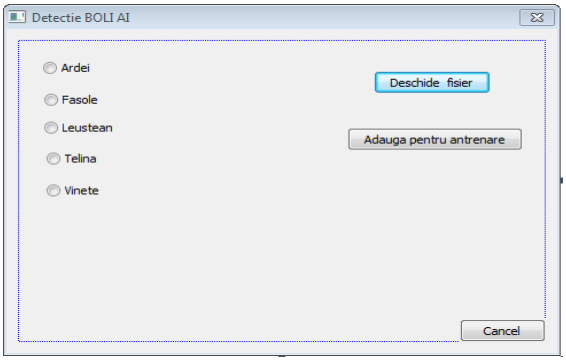

Fig. 2. *Program interface*

The developed model must solve both the classification problem - displaying the class of diseases - and the problem of positioning the object in the image to confirm to the user that the operation is successful (Fig. 5).

There are specific diseases that impose special challenges, especially those that present very small surfaces with a geometry that can easily be confused with the chromatic structure of the leaves (Fig. 3). To train the neural network, we used sets of our own images taken from culture. Unlike several approaches of other groups of researchers, who used training sets with backgrounds from the laboratory, the algorithm uses images from its own culture for training, where the background is a natural one. This allows more

THE ANNALS OF "DUNAREA DE JOS" UNIVERSITY OF GALATI
FASCICLE IX. METALLURGY AND MATERIALS SCIENCE
Nº. 3 - 2022, ISSN 2668-4748; e-ISSN 2668-4756
Article DOI: https://doi.org/10.35219/mms.2022.3.04

training data to be entered and allows the platform to have the option to enter new training data.

The size of the images for training the neural network is 120 x 120 pixels. The number of images is in range of 80-200 images varying on each disease. In addition, for each data set, 20% more training images from the original set were generated by augmentation (rotation and dimming). The platform allows a new image entered by the user to be used for learning.

This was done to increase the training set and eliminate identification errors related to the positioning of the plant relative to the camera.

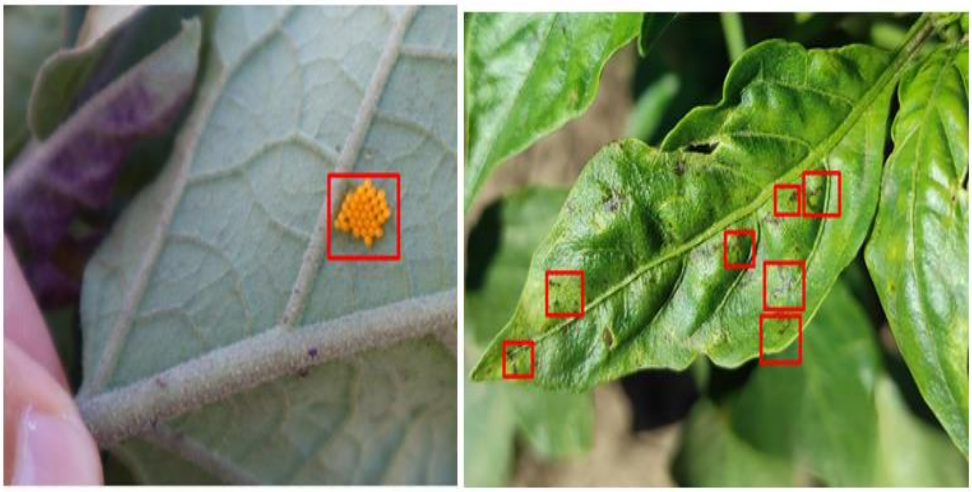

Fig. 3. *Identification of disease*

For testing, 50 images were used for each of the diseases indicated in this program testing platform. The precision detection is shown in Table 2.

Table 2.

Pepper	Precision[%]	Beans	Precision[%]
Myzus persicae	80	Tetranicus urticae	98
Fusaium oxisporum	99	Colletotrichum lindemuthianum	98
Xanthomonas vesicatorie	99	Xanthomonas campestris	99
Alternaria tenuis	98		
Tabacco mosaic virus in pepper	93		
Alfalfa mosaic virus in pepper	92		
Lovage	Precision[%]	Celery	Precision[%]
Euleia heraclei	99	Cercospora apii	89
Septoria apiicola	93	Septoria petroselini	79
Eggplants	Precision[%]		
Leptinotarsa decemlineata- adult	86		
Leptinotarsa decemlineata- larve	87		
Leptinotarsa decemlineata- egg	85		

It is important to note that although CNN architectures are powerful in classification, segmentation, and object detection tasks, they require a large amount of data to be trained.

Fig. 4. *Reduced size disease*

The platform allows a new image entered by the user to be used for learning. This usually requires large amounts of data, but this can be mitigated using methods such as filters associated with multiple disease classes. Identifying diseases with a point-like appearance, from a colour point of view resembling the leaf is a particular challenge. However, the algorithm allows recognition with a good detection rate (Fig. 4).

THE ANNALS OF "DUNAREA DE JOS" UNIVERSITY OF GALATI
FASCICLE IX. METALLURGY AND MATERIALS SCIENCE
Nº. 3 - 2022, ISSN 2668-4748; e-ISSN 2668-4756
Article DOI: https://doi.org/10.35219/mms.2022.3.04

Fig. 5. *Detection of disease location*

3. Conclusions

There are various approaches to solve the problem of disease identification with the help of artificial intelligence algorithms. However, there is still no effective solution.

The team developed an intelligent platform capable of identifying 17 classes of diseases using images of plants with healthy and diseased leaves. To train and test models, we used our own data set with a relatively small number of images, and all images were captured in culture, and not in laboratory conditions. This presents multiple advantages and shows the robustness of the identification algorithm. After splitting the dataset into training images and testing images we achieved the best accuracy rate of 99% and it took 400 iterations to train the network with images.

Acknowledgement

The investigations were financial supported by the research ADER 25.2.2, Cercetare cu privire la proiectarea unui echipament inteligent horticol de analiza, predictiva si analiza biodinamica.

References

[1]. Akhtar A., Khanum A., Khan S. A., Shaukat A., *Automated Plant Disease Analysis: Performance comparison of machine learning techniques*, (In) Eleventh International Conference on Frontiers of Information Technology, IEEE, p. 60-65, 2013.

[2]. Amara J., Bouaziz B., Algergawy A., *A deep learnin gbased approach for banana leaf diseases classification*, (In) Proceedings of Datenbanksysteme für Business, Technologie und Web (BTW 2017) – Workshop Bonn: Gesellschaft für Informatik, 2017.

[3]. Arivazhagan S., Shebia R. N., Ananthi S., Varthini S. V., *Detection of unhealthy region of plant leaves and classification of plant leaf diseases using texture features*, Agricultural Engineering International: CIGR Journal 15, 2013.

[4]. Arivazhagan S., Ligi S. V., *Mango Leaf Diseases Identification Using Convolutional Neural Network*, International Journal of Pure and Applied Mathematics, 2018.

[5]. Atila M., Uar M., Akyol K., Uar E., *Plant leaf disease classification using efficientnet deep learning model*, Ecol Inform. 2021.

[6]. Sabrol H., Kumar S., *Recent studies of image and soft computing techniques for plant disease recognition and classification*, Int J Comput Appl., 2015.

[7]. Yalcin H., Razavi S., *Plant classification using convolutional neural networks*, In: 2016 5th international conference on agro-geoinformatics (agro-geoinformatics), New York: IEEE, 2016.

[8]. Fuentes A., Lee J., Lee Y., Yoon S., Park D. S., *Anomaly detection of plant diseases and insects using convolutional neural networks*, In: ELSEVIER conference ISEM 2017-The International Society for Ecological Modelling Global Conference, 2017.

[9]. Hasan M. J., Mahbub S., Alom M. S., Nasim M. A., *Rice disease identification and classification by integrating support vector machine with deep convolutional neural network*, In: 2019 1st International conference on advances in science, engineering and robotics technology (ICASERT), 2019.

[10]. Thenmozhi K., Reddy U. S., *Crop pest classification based on deep convolutional neural network and transfer learning*, Comput Electron Agric., 2019.

[11]. Fang T., Chen P., Zhang J., Wang B., *Crop leaf disease grade identification based on an improved convolutional neural network*, J Electron Imaging, 2020.

THE ANNALS OF "DUNAREA DE JOS" UNIVERSITY OF GALATI
FASCICLE IX. METALLURGY AND MATERIALS SCIENCE
Nº. 3 - 2022, ISSN 2668-4748; e-ISSN 2668-4756
Article DOI: https://doi.org/10.35219/mms.2022.3.05

REDUCING GAS EMISSIONS FROM TRANSPORT BY INTRODUCING HYBRID ELECTRIC VEHICLES

Mariana LUPCHIAN
"Dunarea de Jos" University of Galati, Romania
e-mail: mariana.lupchian@ugal.ro

ABSTRACT

The work presents one of the most serious problems related to air pollution as it can have effects both in the short term, but especially in the medium and long term. By increasing the number of automobiles put into circulation every year, in addition to the increase in fuel consumption, the problem of pollution has been accentuated, due to the noxious emissions of the internal combustion engines used for their propulsion. The requirement to reduce fuel consumption has become even more acute as it is closely related to environmental pollution.

KEYWORDS: hybrid electric vehicles, fuel consumption, CO_2 emissions, environmental pollution, plug-in hybrids

1. Introduction

Through the Kyoto Protocol, developed countries committed to reduce greenhouse gas emissions in the period 2008-2012 by approximately 5% compared to 1990 levels.

Hybrid vehicles manage to reduce the consumption of conventional fuel by using the electricity they produce while driving. Although the consumption is lower, the basis of the propulsion of hybrid cars is still a fossil fuel - a non-renewable resource that is running out [3].

Transport was the source of around a quarter of all EU CO_2 emissions in 2019. Of these, 71.7% came from road transport, according to a report by the European Environment Agency.

The new Framework Directive (Directive 2007/46/EC1) extends the legislative framework for the type approval of motor vehicles, including all types of vehicles, regardless of the propulsion systems used.

The new Framework Directive also includes hybrid electric vehicles and electric vehicles [4].

Directive 2009/33/CE of the European parliament and of the council of 23 April 2009 requires contracting authorities, contracting entities, as well as certain operators to take into account the energy and environmental impact during the lifetime, including energy consumption, CO_2 emissions and of certain pollutants, when purchasing road transport vehicles, with the objectives of promoting and stimulating the market of non-polluting and energy-efficient vehicles and improving the contribution of the transport sector to Community policies in the field of environment, climate and energy [5].

Directive 2010/31/EU states that states must establish requirements for the installation of a minimum number of recharging points for electric vehicles for all non-residential buildings with more than twenty parking spaces by 1 January 2025 [6].

Electric power has the potential to increase the energy efficiency of road vehicles and contribute to a reduction in CO_2 in transport. This is a source of energy indispensable for the introduction of electric vehicles.

The number of recharging points should be set by taking into account the number of electric vehicles expected to be registered by the end of 2020 in each Member State [7].

According to the data provider, APIA, interest in "green" cars (electric and hybrid) continues to remain high this year. In 2018, they held a 2.5% share of the total market. Even if the volumes are still very small, the evolution is extremely encouraging, the increase recorded this year being 225.5% in the electric segment (485 units, in the first 7 months of 2018, compared to only 149 in 2017), respectively +54.5% for hybrids (1,754 units in 2018, compared to 1,135 units in 2017), which proves that there is an increased interest in this category of cars [8].

The European Commission EU 2020 strategy includes the green car initiative "European Green Cars Initiative (EGCI); which consists of a series of measures to support research and innovation in order to create a new generation of cars, trucks and buses,

THE ANNALS OF "DUNAREA DE JOS" UNIVERSITY OF GALATI
FASCICLE IX. METALLURGY AND MATERIALS SCIENCE
Nº. 3 - 2022, ISSN 2668-4748; e-ISSN 2668-4756
Article DOI: https://doi.org/10.35219/mms.2022.3.05

which will protect the environment and create new jobs and a competitive industry.

Harmonization of regulations for car construction is very important [9].

The European Commission's EU 2020 strategy includes the green car initiative "European Green Cars Initiative (EGCI)", which consists of a series of measures to support research and innovation in order to create a new generation of cars, trucks and buses that protect the environment and create new jobs and a competitive industry. In the Multiannual Strategic Plan of the ENIAC platform of the European Commission, two emergencies "full electric car" and "safe car" are included.

In this sense, two E3Car projects were launched in 2009 – Nanoelectronics for an energy efficient electric car and SE2A – Nanoelectronics for Safe, Fuel Efficient and Environment Friendly Automotive Solutions [10].

In order to ensure that hybrid vehicles comply with the noise limits set out in Directive 97/24/EC in all operating modes, it is also necessary to adapt the type approval test procedure used to measure the noise in Directive 97/24/CE [11].

In Romania, according to the statistics provided by the Association of Automobile Manufacturers and Importers (APIA), based on the statistics of the Motor Vehicle Registration and Driving License Regime Directorate (DRPCIV), in the first 10 months of 2021, "electrified" cars, respectively electric ones (100% and plug hybrids – in which they are charged from an external source), as well as full hybrids (cars that also have electric propulsion without charging from the source) have reached a market share of almost 13%, higher about 2 times compared to the previous period in 2020. In November 2021, a market share of 14.2% was already recorded, which is 2.1 times higher than the one they had in the same period last year (6.7%) [12].

The European Union wants at least 30 million vehicles with zero emissions to circulate on its roads by 2030, in order to reduce the consumption of fossil fuels in the member countries. "The EU's goal of zero greenhouse gas emissions by 2050 cannot be achieved without the introduction of extremely ambitious measures to reduce the transport sector's dependence on fossil fuels." Sales of hybrid and electric cars in the European Union and Great Britain reached 458,915 units last year, up 110% compared to 2017 [13].

Car sales in Europe will see a considerable increase for cars equipped with innovative systems that protect the surrounding nature.

2. Hybrid electric vehicles

The use of oil as the sole source of energy for passenger vehicles has led to economic and political crises that have been amplified as the world's oil reserves have dwindled. By increasing the number of cars put into circulation every year, in addition to the increase in fuel consumption, the problem of pollution has increased, due to the emissions of internal combustion engines used for their propulsion.

The development of the car was closely related to the reduction of fuel consumption and the adaptation of the propulsion system to operation with other types of fuels.

The requirement to reduce fuel consumption has become even more acute since it is closely related to environmental pollution.

An alternative would be the use of electric vehicles, the number of which is still not significant.

"Hybrid electric vehicle (HEV) means a vehicle that, in order to ensure its mechanical propulsion, takes energy from the following two stored energy sources on board: a fuel; an electrical energy storage device (e.g., battery, capacitor, flywheel/generator etc.

Electric and electric hybrid cars are superior to conventional ones both in terms of energy conversion efficiency and harmful emissions.

Electric motors offer a range of benefits from reduced emissions while driving, to lower running costs, to more responsive acceleration at start-up.

The main elements of hybrid electric vehicles are the electric motor and the thermal engine, the electric energy source and/or the electric energy storage system, the transmission, the power electronics and the command-and-control systems that ensure the operation of the vehicles as a whole.

Electrified engines are more expensive than gasoline or diesel engines.

Regenerative braking is common in hybrid vehicles. The energy created by the vehicle when braking is saved in the battery. This energy can then be used to power the electric motor or other electricity consuming components [18].

The Electric Vehicles Initiative (EVI) is a forum for global cooperation on the development and deployment of electric vehicles [19].

Charging times vary and depend on factors such as outside temperature, current battery temperature, charging equipment, battery condition, and vehicle condition.

It is predicted that by 2030 there will be no new car without at least one electric motor or without benefiting from a hybrid system. Both electric cars and electric hybrids are criticized for their lack of autonomy [2].

THE ANNALS OF "DUNAREA DE JOS" UNIVERSITY OF GALATI
FASCICLE IX. METALLURGY AND MATERIALS SCIENCE
Nº. 3 - 2022, ISSN 2668-4748; e-ISSN 2668-4756
Article DOI: https://doi.org/10.35219/mms.2022.3.05

The issue of justifying an autonomy comparable to that offered by fossil fuels is raised.

There are solutions that increase the range when needed, such as the "Range Extender" mode.

Plug-in hybrid vehicles (PHEVs) face an uncertain future if the EU reclassifies how CO_2 emissions are measured. If emissions double, owners will pay higher taxes and switch to electric cars.

2.1. Evolution of CO_2 emissions

The European Union is set to impose a new CO_2 directive on hybrid cars (PHEVs), which could have a dramatic impact on their success and accelerate the adoption of electric vehicles.

All PHEVs are likely to have their official emissions figures – measured in grams per kilometre of CO_2 (g/km) – more than double by 2027 under the new EU6 regulations.

A hybrid car works on the basis of two sources of power, a gasoline engine and an electric one. This system has the possibility to recover energy through regenerative braking.

When the car is idling, the number of emissions released into the atmosphere is much higher. However, most drivers believe that stopping and restarting the engine consumes more fuel than idling. This is not true unless the car has been idling for less than a minute. The pollution produced by a car is greater if we also turn on the air conditioning system. This does not mean, however, that we should not benefit from the existence of this system.

Figure 1 shows the evolution of CO_2 emissions in the European Union from 1990 to 2019.

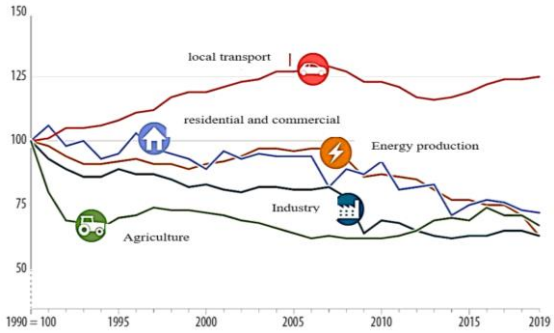

***Fig. 1.** Evolution of CO_2 emissions in the EU (1990-2019)* [16]

The advantages of hybrid propulsion systems are: zero local emissions (electric car); reduced fuel consumption/reduced CO_2 emission due to: recovery of braking energy; start / stop operation; moving the engine operating regimes towards the economic pole, reducing the cylinder capacity through electric assistance [14].

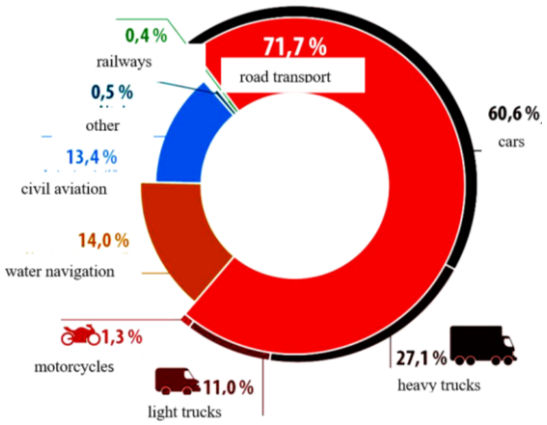

***Fig. 2.** Emissions by transport mode Source: European Environment Agency 2022* [16]

Figure 2 shows gas emissions from transport (2019). Private cars pollute the most, emitting 60.6% of all CO_2 emissions from European road transport [16].

There are two ways to reduce CO_2 emissions in cars: making them more efficient or changing the fuel. In 2019, most road transport in Europe used diesel (66.7%), followed by petrol (24.55%).

Electric cars are gaining ground though. They accounted for 11% of all new vehicle registrations in 2020.

Sales of electric vehicles (full electric or plug-in hybrid) have grown massively since 2017 and tripled in 2020 when the current CO_2 targets came into effect.

Electric vans accounted for 2.3% of the newly registered van market in 2020.

Most people charge their cars at home overnight using a charging wall box. Others have the option of charging their car at work or at public charging stations, which in many areas are becoming easier to find.

The production of an electric car is less environmentally friendly than an internal combustion engine car, and the level of emissions from electric

THE ANNALS OF "DUNAREA DE JOS" UNIVERSITY OF GALATI
FASCICLE IX. METALLURGY AND MATERIALS SCIENCE
Nº. 3 - 2022, ISSN 2668-4748; e-ISSN 2668-4756
Article DOI: https://doi.org/10.35219/mms.2022.3.05

vehicles varies depending on how the electricity is produced.

One of the major problems we are currently facing is the problem of pollution. Emissions during the driving of vehicles play an important role in atmospheric pollution.

Transport was the source of around a quarter of all EU CO_2 emissions in 2019. Of these, 71.7% came from road transport, according to a report by the European Environment Agency.

The state will have to provide the necessary infrastructure for charging stations for electric vehicles and in apartment buildings, both new and those undergoing major renovations, and which have more than ten parking spaces.

Figure 3 shows the evolution of CO_2 emissions from new vehicles.

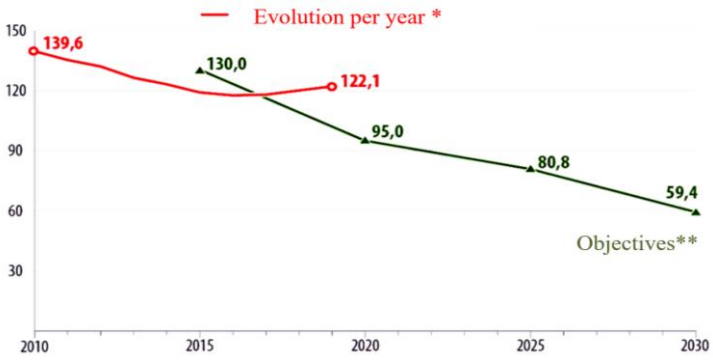

Fig. 3. *The evolution of CO_2 emissions from new vehicles (g CO_2/km)* [16]

*Estimated for 2010, 2011 and 2012
**Indicative objectives calculated by the European Environment Agency (EEA) according to regulation (EU) 2019/63.

Hybrid electric vehicles can be propelled either only by the internal combustion engine, or by the electric one or more, or by all at the same time.

Mild hybrid vehicles are efficient at low speeds. Mild hybrid vehicles suit the urban lifestyle: short trips in the city at relatively low speeds.

The accumulators of a mild hybrid can be charged exclusively with the help of its own systems, that is, the energy sources on board are used. These vehicles cannot be powered by the electric motor alone. Compared to plug-in hybrids, mild hybrid vehicles have smaller motors/generators and smaller capacity batteries, which is reflected in price and performance.

Hybrid electric vehicles have a greater autonomy than mild hybrids, they are intended for longer roads and high speeds.

Electric cars are at least twice as clean as internal combustion ones.

We have to consider four elements: the impact during production, the impact at street level, the energy consumption per hundred kilometres, the sources from which this energy is produced.

According to a study by the Union of Concerned Scientists, the production of an electric car is 15% to 68% more polluting, in terms of CO_2 emissions, than the production of a normal car.

This difference in CO_2 emissions cancels out after several tens of thousands of kilometres of driving an electric car, usually in the first 5 years of use.

Advantages of hybrid cars: hybrid cars must be powered only with fuel (not electricity); the electric current they use is produced while running, by the combustion engine and also from the braking energy; when you apply the brake, the battery is supplied with electricity; hybrid cars do not require a special infrastructure (special fuelling stations) being able to be used wherever there are regular petrol pumps; the cars are very quiet.

Disadvantages of hybrid cars: hybrid cars do not solve the problem of using fossil fuels, they are still based on gasoline, thus contributing to the depletion of these non-renewable resources; they are more expensive.

Designing and building this type of vehicle is more expensive for manufacturers. Although the initial cost is high, a return is achieved over time due to reduced fuel consumption and reduced maintenance.

Autonomy can be a problem if we compare it to that of traditional ones.

Maintenance has a higher cost and cannot be performed in all workshops.

3. Conclusions

One of the major problems we are currently facing is the problem of pollution. Emissions during

THE ANNALS OF "DUNAREA DE JOS" UNIVERSITY OF GALATI
FASCICLE IX. METALLURGY AND MATERIALS SCIENCE
Nº. 3 - 2022, ISSN 2668-4748; e-ISSN 2668-4756
Article DOI: https://doi.org/10.35219/mms.2022.3.05

the driving of vehicles play an important role in atmospheric pollution.

Transport was the source of around a quarter of all EU CO_2 emissions in 2019 (71.7% came from road transport, according to a report by the European Environment Agency).

Reducing CO_2 emissions is important because this gas is part of the category of those that during 2021, the European Commission proposed to reduce the emissions limit for cars and vans by a further 15% from 2025, followed by a 55% reduction for cars and 50% for vans from 2030, and to reach zero emissions by 2035.

Private cars pollute the most, emitting 60.7% of all CO_2 emissions from European transport.

Sales of hybrid and electric cars have increased thanks to tougher new emissions standards.

The global trend is to reduce the pollution generated by classic engines, with internal combustion, which is why most governments encourage drivers to reorient themselves to those that emit as low a level of emissions as possible.

Electric vehicles are already proving to be cleaner than gasoline-powered vehicles. As the share of electricity from renewable sources will increase in the future, electric cars will become even less harmful to the environment.

Electric vehicles would greatly reduce the major causes of smog, substantially eliminate ozone depletion and reduce greenhouse gases. With stricter standards on power plant SO_2 emissions, electric vehicles would have a reduced impact on SO_2 levels.

The major impediments to the widespread acceptance of electric vehicles by the general public are their limited range and lack of infrastructure. The solution to the autonomy problem may come in extensive research and development efforts in batteries, fuel cells and other alternative energy storage devices. An alternative approach is to make people aware of the problem of global warming and the advantages of electric vehicles.

References

[1]. Joldoș C., Șmadici O.-V., *Hybrid propulsion systems an efficient solution for on–board auto vehicle energy*, A XI-a Conferinta Natioanala multidisciplinara-cu participare international, "Profesorul Dorin Pavel-fondatorul hidroenergeticii romanesti", Sebes, 2011.

[2]. Croitorescu V., Negruș E., *Cerințe și reglementări impuse automobilelor hibride electrice*, Lucrările celei de-a VII-a ediții a Conferinței anuale a ASTR, Universitatea "Politehnica" din București, 2019.

[3]. ***, https://www.colegiulasachi.ro/pdf-uri/Prezentare%20motorizare%20hibrid.pdf.

[4]. ***, http://anap.gov.ro/web/wp-content/uploads/2021/07/Comunicarea-COM-2020_C352_01_Directiva-vehicule-curate.pdf.

[5]. ***, http://data.europa.eu/eli/dir/2009/33/oj, Directive 2009/33/EC of the European parliament and of the council of 23 April 2009 on the promotion of non-polluting and energy-efficient road transport vehicles.

[6]. ***, Directive 2010/31/EU of the European parliament and of the council of 19 May 2010 on the energy performance of building.

[7]. ***, Directive 2014/94/UE a parlamentului European și a consiliului din 22 octombrie 2014 privind instalarea infrastructurii pentru combustibili alternativi.

[8]. ***, https://www.gov.ro/ro/print?modul=subpagina&link=nota-de-fundamentare-oug-nr-17-19-03-2019#null.

[9]. ***, https://eur-lex.europa.eu/legal-ontent/RO/TXT/PDF/?uri=CELEX:52012AE2487&from=LV.

[10]. ***, https://www.agir.ro/buletine/2079.pdf.

[11]. ***, https://eur-lex.europa.eu/LexUriServ/LexUriServ.do?uri=OJ:L:2009:213:0010:0025:RO:PDF.

[12]. ***, https://ziare.com/auto/masini-electrice/top-10-cele-mai-vandute-ma-ini-electrice-i-hibride-in-romania-decembrrie-2021-1715232.

[13]. ***, https://www.digi24.ro/stiri/externe/ue/ue-vrea-ca-30-de-milioane-de-masini-cu-zero-emisii-sa-circule-in-europa-pana-in-2030-1412334.

[14]. ***, http://www.gomexpert.ro/satumare/top-stiri/97-sistem-de-propulsie-hibrid-termic-electric.

[15]. ***, https://www.europarl.europa.eu/news/ro/headlines/society/20190313STO31218/emisiile-de-co2-de-la-autovehicule-date-si-cifre-infografic.

[16]. ***, https://www.europarl.europa.eu/news/ro/headlines/society/20190313STO31218/emisiile-de-co2-de-la-autovehicule-date-si-cifre-infografic-Emisiile de CO_2 de la autovehicule: date și cifre (infografic).

[17]. ***, https://www.europarl.europa.eu/news/ro/headlines/society/20190313STO31218/emisiile-de-co2-de-la-autovehicule-date-si-cifre-infografic.

[18]. ***, https://auto.radacini.ro/masinile-hibrid-si-emisiile-co2-5-lucruri-de-stiut/.

[19]. ***, Urs Muntwyler, The Implementing Agreement IA "Hybrid- and Electric Vehicle" of the International Energy Agency (IEA) the international cooperation program with a new record of member countries, World Electric Vehicle Journal Vol. 5 - ISSN 2032-6653, WEVA, 2012.

THE ANNALS OF "DUNAREA DE JOS" UNIVERSITY OF GALATI
FASCICLE IX. METALLURGY AND MATERIALS SCIENCE
No. 3 - 2022, ISSN 2668-4748; e-ISSN 2668-4756
Article DOI: https://doi.org/10.35219/mms.2022.3.06

INCREASE THE LOAD OF LOSS OF STABILITY FOR THE PILLARS OF LARGE-OPENING HALLS

Marius BOTIȘ, Costel PLEȘCAN
Transilvania University of Brasov, Department of Civil Engineering, Romania
e-mail: plescan.costel@unitbv.ro

ABSTRACT

At the ground floor halls with an opening or more, the forces that are transmitted through the pillars due to gravitational loads (snow, and her weight) have high values. The gravitational difference that is transmitted to the pillars increases the greater the opening between the pillars is. In this Article we analyse the pillars of halls that are articulated recessed, because they have the advantage that the joints do not transmit bending moments. In the case of halls with large openings or halls rehabilitated or strengthened, to increase the critical load of loss of stability can increase the moment of inertia of the pillars from the recessed to the articulated end. In this Article, a parametric numerical study is presented, which establishes the critical load at a pillar with a variable section, depending on the length of the area where the moment of inertia of the slat has been increased.

KEYWORDS: Monte Carlo method, moments of inertia of flat surfaces, probabilistic algorithms

1. Introduction

Industrial ground floor halls (Fig. 1) are structural systems in which the axial forces transmitted through the pillars are very high. The first cause of significant values of axial forces is the very large opening between the pillars which leads to large gravitational afferent. Another important cause of increased axial loads in pillars is the existence of bridge cranes. A simple and effective solution to increase the critical load is to increase the moment of inertia of the pillars, starting from the stapling of the pillars in the good foundation ground to the articulated end where the gravitational input from the wraparound flows. Increasing the moment of inertia to newly designed structures is done from the design phase, and the area that is enlarged for optimization is established from the design phase of the structures. For the existing structures to which the destination is changing, due to new loads must be designed mansions of different lengths and with certain moments of inertia to be applied to the pillars of the hall in areas established by calculation. Application of these masons will lead to increased critical loads of loss of stability [1].

2. Theoretical and numerical model

The pillar shown in Fig. 2 is considered to be the static diagram of an articulated-inlay pillar from an industrial hall. For the pillar with the constant cross-section of Fig. 1 the equation of the deformed mean fiber is written on the deformed form, and by solving this equation the critical charge is determined [2].

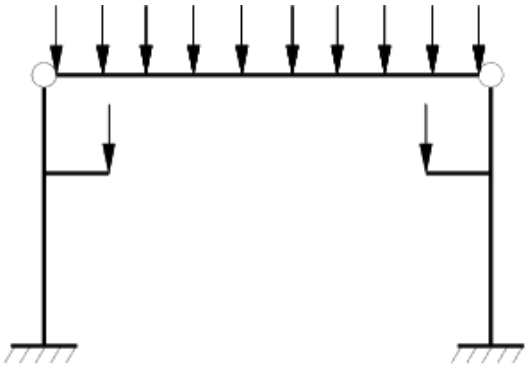

Fig. 1. *Industrial ground floor halls*

THE ANNALS OF "DUNAREA DE JOS" UNIVERSITY OF GALATI
FASCICLE IX. METALLURGY AND MATERIALS SCIENCE
No. 3 - 2022, ISSN 2668-4748; e-ISSN 2668-4756
Article DOI: https://doi.org/10.35219/mms.2022.3.06

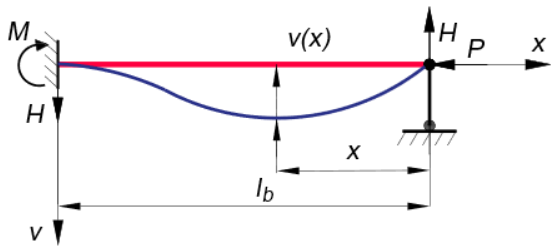

Fig. 2. *Static diagram of an articulated-inlay pillar from an industrial hall*

For a current section of the pillar in Fig. 1, the variation expression of the bending moment at distance x is:

$$M(x) = P \cdot v - H \cdot x$$

From the differential equation of the approximate deformed mid fibre results:

$$\frac{d^2v}{dx^2} = -\frac{M(x)}{EI};$$
$$\frac{d^2v}{dx^2} + \frac{P \cdot v}{EI} = \frac{H \cdot x}{EI};$$
$$k^2 = \frac{P}{EI}$$

The solution of the nonhomogeneous second order differential equation with constant coefficient is:

$$v(x) = v_o(x) + v_p(x);$$
$$v(x) = C_1 \sin(kx) + C_2 \cos(kx);$$
$$v_p(x) = Cx \rightarrow \frac{P \cdot v_p}{EI} = \frac{H \cdot x}{EI};$$
$$v_p = \frac{H}{P} \cdot x$$

The general solution of the differential equation is:

$$v(x) = C\_1 \ sin\,(kx) + C\_2 \ cos\,(kx) + H/P \cdot x;$$
$$v^{\wedge\prime}(x) = C\_1\, k\, cos\,(kx) - C\_2\, k\, sin\,(kx) + H/P$$

The constants of integration are determined from the conditions of existence of the deformed form as the form of equilibrium:

x = 0;
v(0) = 0;
C_2 = 0;
x = l;
v(l) = 0;
x = l;
v^\' (l) = 0.

After applying the limit conditions, the homogeneous system of equations is obtained:

$$\begin{cases} C_1 \sin(kl) + \frac{H}{P} l = 0; \\ C_1 k \cos(kl) + \frac{H}{P} = 0. \end{cases}$$

The unknowns of the system of equations (5) are C1 and H/P, the homogeneous system of equations has non-trivial solutions if the determinant of the coefficients is zero.

$$\begin{vmatrix} \sin(kl) & l \\ k\cos(kl) & 1 \end{vmatrix} = 0;$$
$$\sin(kl) - kl\cos(kl) = 0;$$
$$\mathrm{tg}(kl) = kl;$$
$$kl = 4{,}493;$$
$$(kl)^2 = \left(\frac{\pi}{0{,}699}\right)^2;$$
$$P_{cr} = \frac{\pi^2 EI}{(0{,}699l)^2}$$

To analyse pillars with a variable moment of inertia along the bar, consider the pillar of Fig. 3, which consists of two zones, one with the moment of inertia I and the other with the moment of inertia 2I.

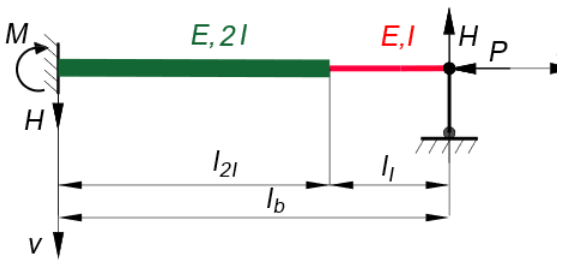

Fig. 3. *The two zones of the pillar*

To determine the critical load of the column for different ratios between the area with the moment of inertia I and 2I, a Matlab program was created that determines the critical load for loss of stability by the finite element method. The program is based on the stability equation, which for a structure has the form [2]:

$$det\left|\,[K_{el}] - \lambda[K_g]\right| = 0.$$

where:

$[K_{el}]$ is the matrix of elastic stiffness of

THE ANNALS OF "DUNAREA DE JOS" UNIVERSITY OF GALATI
FASCICLE IX. METALLURGY AND MATERIALS SCIENCE
No. 3 - 2022, ISSN 2668-4748; e-ISSN 2668-4756
Article DOI: https://doi.org/10.35219/mms.2022.3.06

structures that is also used in the first-order calculation of structures

$[K_g]$ is the geometric matrix of the structure.

By solving the stability equation, the eigenvalues λ_(i,) i=1,2,3… are obtained. The minimum value λ_min represents the multiplication factor that is applied to the axial force determined from a first-order calculation.

There are cases when the increase of the moment of inertia of the column is difficult to achieve from the embedment towards the free end of the column, because the muff to be applied must be designed so that the foundation takes the capable moment of the muff. To avoid this inconvenience, the muff can be applied inside the pillar. This avoids the end areas which are areas whose grips are already calculated and conformed. Fig. 4 shows a pillar with a muff applied in the middle.

For different values of the length of the muff, the critical force for loss of pillar stability can be determined. By increasing the length or the moment of inertia for the muff, the critical force can be increased up to the required value. The solution with the muff in the middle is more practical and easier to achieve than the solution with a muff that starts from the recess. The main advantage of a reinforced hall with a muff in the middle is represented by the fact that the muff can be applied without dismantling the hall and stopping the technological processes taking place inside the hall. For ease of assembly and execution, the muff is made of two half-pieces that are welded together. To fix the muff on the pillar, the ends of the muff are welded to the pillar of the hall.

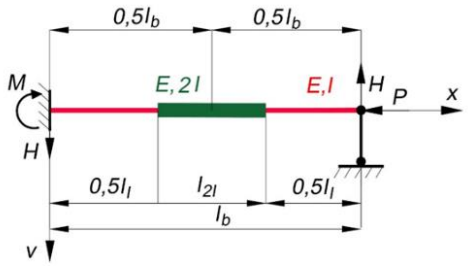

Fig. 4. *pillar with a muff applied in the middle*

3. Results and conclusions

To highlight the increase of the critical force in the bar with variable section from the embedment to the free end Fig. 3, a pillar with a length of 8 m articulated-embedded made of steel with E = 2.1·10^5 MPa, was analyzed, with the ring cross-section with outer diameter D = 100 mm and the inner diameter d = 50 mm.

For different values of the ratio between the length of the zone with moment 2I - l2I and the length of the zone with inertia moment I - li the ratio of the critical force at the bar with variable section to the critical force at the bar with constant section is shown in Fig. 4.

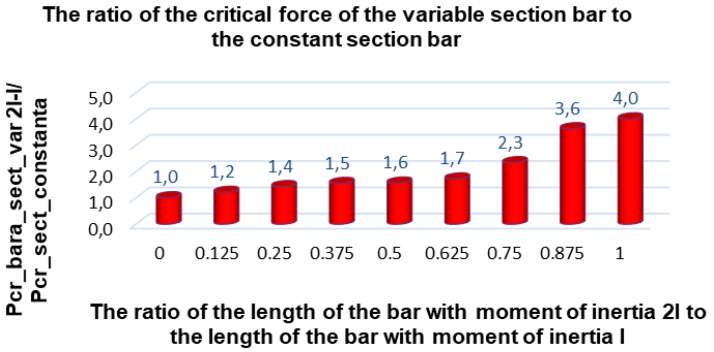

Fig. 5. *The critical force at the bar with variable section to the critical force at the bar with constant section*

From the analysis of the results obtained, it follows:

As the length of the zone with inertia moment 2I increases, an increase in the values of the critical force of loss of stability can be observed.

If the entire pillar is considered with the moment of inertia 2I or I, the critical force calculated with the relation of Euler is obtained, which validates the calculation program and implicitly the results from the numerical study.

In the case of the pillar with a muff in the middle of Fig. 4, a parametric study was carried out on how the critical force increases depending on the ratio between the length of the muff l2I with the moment of inertia 2I and the bar of length II with the moment of inertia I. The study was carried out on an

THE ANNALS OF "DUNAREA DE JOS" UNIVERSITY OF GALATI
FASCICLE IX. METALLURGY AND MATERIALS SCIENCE
No. 3 - 2022, ISSN 2668-4748; e-ISSN 2668-4756
Article DOI: https://doi.org/10.35219/mms.2022.3.06

8 m long hinged-recessed pole made of steel with E = 2.1·10^5 MPa, having an annular cross-section with outer diameter D = 100 mm and inner diameter d = 50 mm.

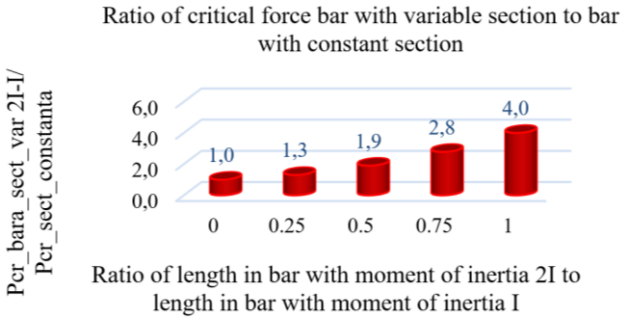

Fig. 6. *Ratio of critical force bar with variable section to bar with constant section*

Based on the results represented in Fig. 6, it follows:

- with the increase of the area with moment of inertia 2I, the critical force of loss of stability increases.

- for the case when the length of the sleeve is the same as the length of the bar, Euler's relationship for calculating the critical load is obtained, a fact that validates the numerical program for calculating the simulation of the loss of stability.

References

[1]. Ruocco E., Wang C., Zhang H., Challamel N., *An approximate model for optimizing Bernoulli columns against buckling*, Engineering Structures, vol. 141, p. 316-327, 2017.
2. Bănuț V., Teodorescu M. E., *Calculul geometric neliniar al structurilor de rezistență*, București: Cospress, 2010.

THE ANNALS OF "DUNAREA DE JOS" UNIVERSITY OF GALATI
FASCICLE IX. METALLURGY AND MATERIALS SCIENCE
No. 3 - 2022, ISSN 2668-4748; e-ISSN 2668-4756
Article DOI: https://doi.org/10.35219/mms.2022.3.07

THE PROBABILISTIC METHOD FOR DETERMINATION THE INERTIA CHARACTERISTICS OF 3D BODIES WITH MONTE CARLO ALGORITHMS

Marius BOTIȘ, Costel PLEȘCAN
Transilvania University of Brasov, Department of Civil Engineering, Romania
e-mail: plescan.costel@unitbv.ro

ABSTRACT

This study determines the inertial characteristics of bodies with probabilistic algorithms of the Monte Carlo type. To determine the mechanical moments of inertia in the case of three-dimensional bodies, the bodies are decomposed into simple bodies for which the moments of inertia are calculated, which are added to Steiner's relations. If the bodies have complex shapes to determine the moments of mechanical inertia, numerical or probabilistic algorithms can be used. This paper presents the main stages in the use of probabilistic algorithms for calculating moments of inertia and finally a program in MATLAB that allows determining the moments of inertia for bodies.

KEYWORDS: Monte Carlo method, moments of inertia of three-dimensional bodies, probabilistic algorithms

1. Introduction

To determine the moments of inertia of the three-dimensional bodies with the Monte Carlo type algorithm, we start from the calculation relations of the moments of inertia in the case of a system of concentrated masses distributed in space.

In the case of a system of n-concentrated masses located in space, the tensor of the mechanical moments of inertia (Billingsley, 2018) is determined starting from the definition relations of the mechanical moments of inertia.

Axial mechanical moments of inertia with respect to the x y and z axis:

Axial mechanical moments of inertia with respect to the x y and z axis:

$$\mathbf{J_{xx}} = \int_{\mathbf{A}} (\mathbf{y^2} + \mathbf{z^2})\mathbf{dm} = \sum_{\mathbf{i=1}}^{\mathbf{n}} \mathbf{m_i}(\mathbf{y_i^2} + \mathbf{z_i^2});$$

$$J_{yy} = \int_A (x^2 + z^2)dm = \sum_{i=1}^{n} m_i(x_i^2 + z_i^2);$$

$$J_{zz} = \int_A (x^2 + y^2)dm = \sum_{i=1}^{n} m_i(x_i^2 + y_i^2)$$

Centrifugal moment of inertia:

$$J_{xy} = \int_A xydm = \sum_{i=1}^{n} m_i x_i y_i .$$

$$J_{xz} = \int_A xzdm = \sum_{i=1}^{n} m_i x_i z_i ;$$

$$J_{yz} = \int_A yzdm = \sum_{i=1}^{n} m_i y_i z_i;$$

The inertia tensor of the mechanical moments of inertia in matrix form becomes:

$$[J] = \begin{bmatrix} \sum_{i=1}^{n} m_i(y_i^2 + z_i^2) & -\sum_{i=1}^{n} m_i x_i y_i & -\sum_{i=1}^{n} m_i x_i z_i \\ -\sum_{i=1}^{n} m_i x_i y_i & \sum_{i=1}^{n} m_i(x_i^2 + z_i^2) & -\sum_{i=1}^{n} m_i y_i z_i \\ -\sum_{i=1}^{n} m_i x_i z_i & -\sum_{i=1}^{n} m_i y_i z_i & \sum_{i=1}^{n} m_i(y_i^2 + x_i^2) \end{bmatrix}$$

Similarly, the tensor of the geometric moments of inertia is determined, which in the form of a matrix becomes:

THE ANNALS OF "DUNAREA DE JOS" UNIVERSITY OF GALATI
FASCICLE IX. METALLURGY AND MATERIALS SCIENCE
No. 3 - 2022, ISSN 2668-4748; e-ISSN 2668-4756
Article DOI: https://doi.org/10.35219/mms.2022.3.07

$$[I]=\begin{bmatrix}\sum_{i=1}^{n}V_i(y_i^2+z_i^2) & -\sum_{i=1}^{n}V_i x_i y_i & -\sum_{i=1}^{n}V_i x_i z_i\\ -\sum_{i=1}^{n}V_i x_i y_i & \sum_{i=1}^{n}V_i(x_i^2+z_i^2) & -\sum_{i=1}^{n}V_i y_i z_i\\ -\sum_{i=1}^{n}V_i x_i z_i & -\sum_{i=1}^{n}V_i y_i z_i & \sum_{i=1}^{n}V_i(y_i^2+x_i^2)\end{bmatrix}$$

From the established relations (3) and (4) it can be observed that the knowledge of the tensor of the geometric moments of inertia also implies the knowledge of the tensor of the geometric moments of inertia.

$$[J]=\rho[I]$$

2. The algorithm for calculating the moments of inertia with the Monte Carlo method

If we know how to calculate the mechanical and geometric moments of inertia for a system of concentrated masses, we can explain how to calculate the geometric and mechanical inertia tensor with the Monte Carlo method.

For the calculation of the moments of inertia for three-dimensional bodies with the Monte Carlo method, infinitesimal masses that are calculated with the following equation.

$$dm=\frac{M}{N}$$

- N is the number of probabilistically generated points in the surface domain for which the moments of inertia are determined;

- M the total mass of the surface.

The higher the number of points generated on the surface domain, the higher the probability of tending to the exact solution. By using the Monte Carlo algorithm, the calculation relations for the mechanical inertia tensor and the geometric inertia tensor become.

Tensor of mechanical moment inertia:

$$[J]=\begin{bmatrix}\sum_{i=1}^{n}dm(y_i^2+z_i^2) & -\sum_{i=1}^{n}dm x_i y_i & -\sum_{i=1}^{n}dm x_i z_i\\ -\sum_{i=1}^{n}dm x_i y_i & \sum_{i=1}^{n}dm(x_i^2+z_i^2) & -\sum_{i=1}^{n}dm y_i z_i\\ -\sum_{i=1}^{n}dm x_i z_i & -\sum_{i=1}^{n}dm y_i z_i & \sum_{i=1}^{n}dm(y_i^2+x_i^2)\end{bmatrix}$$

Tensor of geometric moments of inertia:

$$[I]=\begin{bmatrix}\sum_{i=1}^{n}dV(y_i^2+z_i^2) & -\sum_{i=1}^{n}dV x_i y_i & -\sum_{i=1}^{n}dV x_i z_i\\ -\sum_{i=1}^{n}dV x_i y_i & \sum_{i=1}^{n}dV(x_i^2+z_i^2) & -\sum_{i=1}^{n}dV y_i z_i\\ -\sum_{i=1}^{n}dV x_i z_i & -\sum_{i=1}^{n}dV y_i z_i & \sum_{i=1}^{n}dV(y_i^2+x_i^2)\end{bmatrix}$$

where:

- x_i, y_i, z_i are the coordinates of the concentrated masses dm.

- V is the volume delimited by the three-dimensional body for which the inertia tensor and the geometric tensor are determined.

3. Presentation of MATLAB programs for calculating inertia tensors using the Monte Carlo method

To determine the efficiency of Monte Carlo type algorithms, the moments of inertia will be determined for a cube. In the cases analysed, the moments of inertia will be determined both probabilistically and with exact methods. The following analysis was performed to compare the results obtained analytically with the results obtained with algorithms such as Monte Carlo probabilistic algorithm.

3.1. Implementing the Monte Carlo algorithm in MATLAB for a cube

Matlab code implementation of the Monte Carlo method [2] for determining the moments of inertia for a square of mass M, the axial moments of inertia and the centrifugal moment of inertia for a square have the analytical expressions below:

Axial moments of inertia:

$$I_{yy}=I_{xx}=\frac{2}{3}Ma^2$$

Centrifugal moment of inertia:

$$I_{xy}=-\frac{1}{4}Ma^2$$

Below is a Matlab [3] code for determining the moments of inertia for a cube with side a and mass M. A program for calculating the inertia tensor in Python code is presented in [4].

```
%Calculation of moments of inertia for a cube:
clear;clf;
%Monte Carlo probabilistic algorithm
mass_cube=1;
edge=0.5;
```

THE ANNALS OF "DUNAREA DE JOS" UNIVERSITY OF GALATI
FASCICLE IX. METALLURGY AND MATERIALS SCIENCE
Nº. 3 - 2022, ISSN 2668-4748; e-ISSN 2668-4756
Article DOI: https://doi.org/10.35219/mms.2022.3.07

```
n_mass=10000;
dm_point=mass_cube/n_mass;
Ixx_mc=0;Ixy_mc=0;n=0;
while n<n_mass
x_range=edge*rand;y_range=edge*rand;z_rang
e=edge*rand;
scatter3(x_range,y_range,z_range,30,'MarkerEd
geColor',[0 0 0],...
        'MarkerFaceColor',[1 0 0],...
        'LineWidth',2)
hold on;
rtemp=[x_range y_range z_range];
Ixx_mc=Ixx_mc+dm_point*(x_range^2+z_rang
e^2);
Ixy_mc=Ixy_mc-dm_point*(x_range*y_range);
n=n+1;
end
hold off;
%Theoretical values
Ixxt=2/3*mass_cube*edge^2;
Ixyt=-1/4*mass_cube*edge^2;
Ixx_mc
Ixxt
Ixy_mc
Ixyt
```

Following the analysis, the results presented in Fig. 1 and Fig. 2 were obtained, which are compared with the analytical results obtained.

- For 600 randomly generated points Fig. 1, the theoretical and probabilistic results are:

Theoretical value of moment of inertia
Ixxt = 0.1667
Value moment of inertia with Monte Carlo
Ixx= 0.1720
Theoretical value of moment of inertia
Iyyt =0.1667
Value moment of inertia with Monte Carlo
Iyy= 0.1682
Theoretical value of moment of inertia
Ixyt = -0.0625
Value moment of inertia with Monte Carlo
Ixy= -0.0625

- For 10000 randomly generated points Fig. 2, the theoretical and probabilistic results are:

Theoretical value of moment of inertia
Ixxt = 0.1667
Value moment of inertia with Monte Carlo
Ixx= 0.1655
Theoretical value of moment of inertia
Iyyt =0.1667
Value moment of inertia with Monte Carlo
Iyy= 0.1635
Theoretical value of moment of inertia
Ixyt = -0.0625
Value moment of inertia with Monte Carlo
Ixy= -0.0629

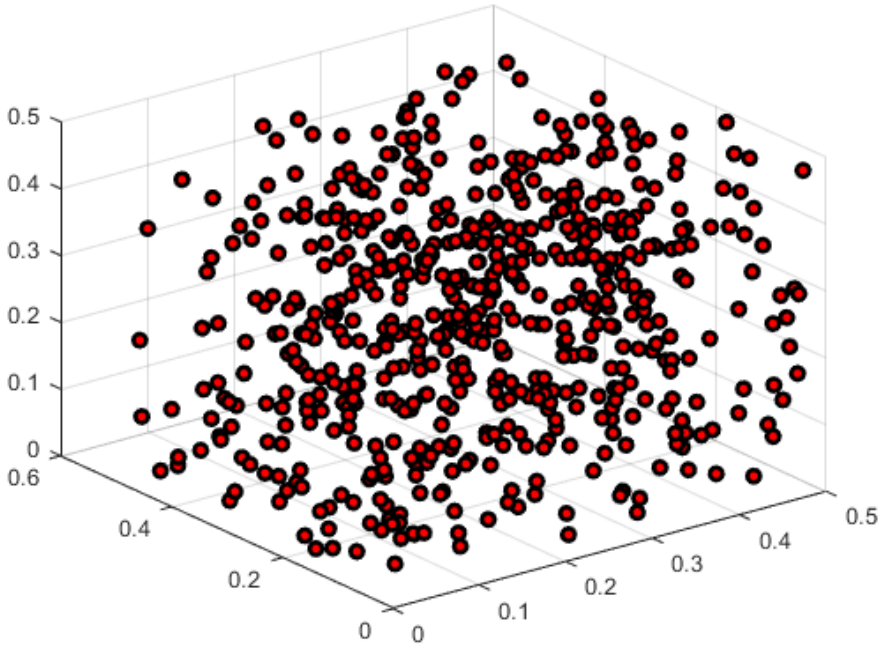

Fig. 1. *Generating 600 points randomly*

THE ANNALS OF "DUNAREA DE JOS" UNIVERSITY OF GALATI
FASCICLE IX. METALLURGY AND MATERIALS SCIENCE
Nº. 3 - 2022, ISSN 2668-4748; e-ISSN 2668-4756
Article DOI: https://doi.org/10.35219/mms.2022.3.07

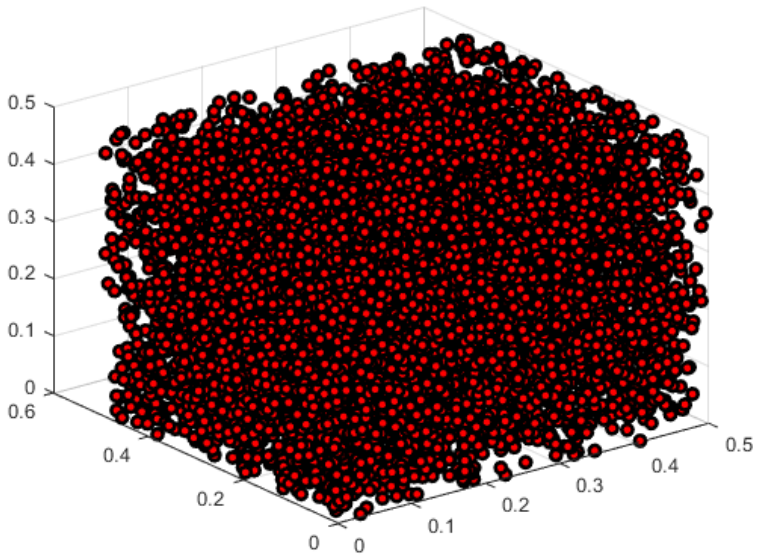

Fig. 2. *Generating 10000 points randomly*

4. Results and conclusions

The analysis of the obtained results shows:

- the Monte Carlo method generates solutions that have a probabilistic character;
- in the calculation of the inertia tensor, the result depends on the number of masses generated in the field occupied by the analysed body;
- the method can be applied if the geometric shape of the body is complex and the calculation with exact methods becomes difficult.

To determine the inertia tensor in the case of flat surfaces, the calculation algorithm is presented in the paper [5].

References

[1]. Billingsley J., *Essentials of Dynamics and Vibration*, Publishing House Springer, 2018.
[2]. Barbu A., Zhu S., *Monte Carlo Methods*, Publishing House Springer ,2020.
[3]. ***, https://www.mathworks.com/products/matlab.html, accessed: 22.00.2021.
[4]. ***, https://www.youtube.com/watch?v=SbTSATs-DBA.
[5]. Botiș M., Pleșcan C., *Matlab Program for Determining the Inertia Characteristics of Flat Surfaces with Monte Carlo Algorithms*, The Annals of "Dunarea De Jos" University of Galati, p. 22-26, June 2022.

THE ANNALS OF "DUNAREA DE JOS" UNIVERSITY OF GALATI
FASCICLE IX. METALLURGY AND MATERIALS SCIENCE
N°. 3 - 2022, ISSN 2668-4748; e-ISSN 2668-4756
Article DOI: https://doi.org/10.35219/mms.2022.3.08

LAMINATED COMPOSITE MATERIALS OBTAINED BY LAMINATION WITH CARBON FIBER

Razvan Andrei IERNUTAN
Technical University of Cluj-Napoca, Faculty of Civil Engineering, Romania
e-mail: razvan.iernutan@ccm.utcluj.ro

ABSTRACT

Composite materials have had a rapid development in recent decades and have come to be used in various fields of industry, including civil engineering. The study of composite materials, but especially of those layered with fibers of different types, is based on improving the physical and mechanical properties and increasing the resistance of the resulting new materials. Through the experimental study, it is aimed to resolve some technological issues regarding the manufacture of samples from composite materials reinforced with carbon fiber and epoxy resins and to improve the mechanical resistance of the usual construction materials from the composition of resistance structures. Combining or reinforcing materials such as wood or concrete, with carbon fiber or glass laminated with epoxy resins or inserted directly into their composition as dispersed reinforcement, increases their properties. In this way, smaller dimensions of the elements can be obtained, leading to an increase in their load-bearing capacity. In this experimental work it is aimed to increase the mechanical and physical resistance behavior of certain materials with the help of carbon fiber laminated with epoxy resins. It has been chosen to use as raw material for samples: concrete, solid brick sandwich, wood, and extruded polystyrene. Depending on the utility of each, after lamination with carbon fibers, the samples are tested for bending moment, compression, fire resistance and shock resistance.

KEYWORDS: composite materials, carbon fibers, matrix, resistance

1. Introduction

Composite materials have appeared due to new demands in several technical fields determined by their rapid progress in the last century. Although this type of material has its origins since antiquity, we will go directly to the modern ones that came into use in the 1940s, reaching the form we know today, consisting of a polymer matrix reinforced with different types of fibres.

They were first used on a large scale in the aeronautical and naval industries. After the war they were also used in nuclear and space projects. As humanity approached the third millennium, composite materials began to be used in more and more fields, including the chemical, automotive, energy industry and, also in construction. Regardless of the technological area that uses these materials, they all follow the same mechanical, physical and chemical properties, which are difficult to achieve today. The aim of this paper is to highlight and analyse these special properties in the present experimental work.

2. Theoretical presentation

2.1. General aspects

2.1.1. Fibbers

fibres are one of the basic components of a composite material. It is a modern raw material, obtained through a complex technological process, hence its high price. Its properties are a determining factor in the behavior of the composite material because they act like a reinforcement, taking over the efforts to which the finished product is subjected.

The basic unit (Fig. 1) represented in the form of a cube that has an atom in each corner, and its sides represent the bonds between atoms [1-3].

THE ANNALS OF "DUNAREA DE JOS" UNIVERSITY OF GALATI
FASCICLE IX. METALLURGY AND MATERIALS SCIENCE
Nº. 3 - 2022, ISSN 2668-4748; e-ISSN 2668-4756
Article DOI: https://doi.org/10.35219/mms.2022.3.08

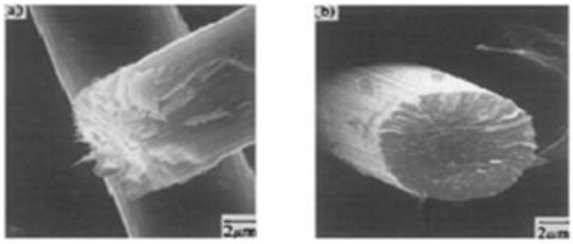

Fig. 1. *Basic unit*

This unit dictates the behavior of the fibres. Being an anisotropic material, its properties differ depending on the direction. The interatomic bonds in the composition of the fibres give it a very rigid and stress-resistant direction of stress, while all other directions are much weaker. This configuration gives properties dependence on the strong direction (ex.: thermal conductivity, electrical etc.) [4, 5].

The fibres are between 3-10 μm thick and the length depends on the type of fiber. In the first stage of processing, at the inter- atomically, the basic units, presented in the previous chapter, are randomly oriented (Fig. 2), offering an isotropic characteristic and resistances equal to those determined by the weakest directions. To obtain the finished product, the raw material is processed into fibres (by stretching), orienting the basic units in the direction of maximum strength and rigidity (Fig. 2). The fiber thus becomes an anisotropic material, clearly superior to the raw material in bulk and with strong resistances in the longitudinal direction [1, 4, 5].

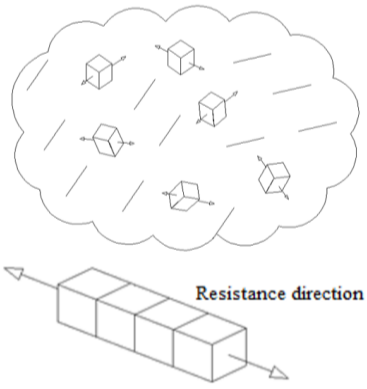

Fig. 2. *Resistance direction of fibers*

2.1.2. Carbon fibers

In nature, carbon is found in different forms, in organic and inorganic compounds. Carbon fiber was discovered in 1879 by Edison, but its industrial production began only in 1960, following a process developed by William Watt, for Royal Aircraft UK.

For a long time, their implementation was problematic, and the recipe for their production is constantly being improved. Carbon fibres appeared as a replacement for glass fiber, acting as reinforcement for a series of materials used in many fields and due to their properties: low density, chemical resistance, mechanical resistance, ease of being put into work and to be moulded in any form. The main disadvantage of fiberglass is their relatively high modulus of elasticity, which causes a fiberglass beam to buckle four times more than a similar steel beam. In restoration, carbon fibres are used in strengthening by plating some structural elements. Cladding with fiber fabrics consists in applying oriented structures characterized by the number of knots per square centimetre, the dimensions and the type of mesh on the surface of masonry, concrete, wood.

It should be mentioned that the fabrics are made of continuous fibres. These are structures with long lengths and small sections, which, due to the parallel ordering of molecules or crystalline domains, have a good mechanical resistance, as well as a high degree of impermeability. The binders used are various epoxy resins that adhere to the surface of the reinforced element and uniformly embed the carbon fabric. These resins must be strong and rigid enough to transfer the forces between the carbon fiber veneer and the protected element. The resulting material - CFRP (Carbon Fiber Reinforced Plastic) - has the following advantages: it is strong, resistant to the chemical attack of acids and bases, it is lighter than glass-based materials, non-magnetic, etc. Some carbon-based materials have strengths of over 3500 N/mm^2 – eight times that of steel bars and with a stiffness comparable to that of steel [1, 4, 5].

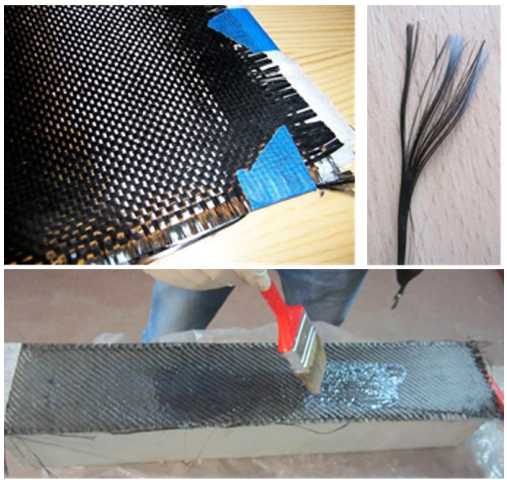

Fig. 3. *Carbon fibres*

There are also some disadvantages. Carbon, like steel, conducts electricity. The epoxy resins in the composition of the material lose their resistance at

THE ANNALS OF "DUNAREA DE JOS" UNIVERSITY OF GALATI
FASCICLE IX. METALLURGY AND MATERIALS SCIENCE
No. 3 - 2022, ISSN 2668-4748; e-ISSN 2668-4756
Article DOI: https://doi.org/10.35219/mms.2022.3.08

certain temperatures, even if they recover with the disappearance of the heat source. Therefore, carbon fiber reinforcement is an additional measure intended to ensure resistance to occasional loads such as earthquakes, in the event of a fire, the existing structures have the possibility to self-sustain for a time regulated by the function they shelter.

At present, CFRP materials are gaining wider acceptance as installation standards begin to emerge. The advantages of using carbon fiber-based materials in restoration and rehabilitation are numerous.

By consolidating with fibres, the structural elements will not have to be intervened except at the superficial level of the plaster, therefore it is not an invasive method and can be largely reversible. In general, it is not necessary to abandon the building by those who occupy it (only if the condition of the construction represents a danger), and the time required for the intervention is much shorter than in the case of other alternative procedures [1-3].

2.1.3. Matrix

To put the fibres mentioned in the previous chapter into operation, it is necessary to consider their arrangement in the appropriate direction, their fixation on the required element and the way of transmitting the efforts in the element to the fibres. These conditions are fulfilled by the matrix. The matrix is the second basic component of the composite material. The matrix is a plastic mass that encloses the fibres, after they have been placed in the correct position. Some types of fibres come in the form of "towels", which represent a strand of fibres, with the aim of facilitating installation.

The role of the matrix is to penetrate through this bundle of fibres until it reaches to include most of the fibres in its mass. Through this adhesion between the element, matrix and fibres, the transfer of efforts can be made, with the help of forces. They stress the fiber axially, introducing forces in the opposite direction (Fig. 4). These stresses are present along the entire length of the fibres, their intensity varies depending on the section in which they are analysed (for e.g.: at the ends, in the middle, etc.). In this way the fiber can absorb the stresses.

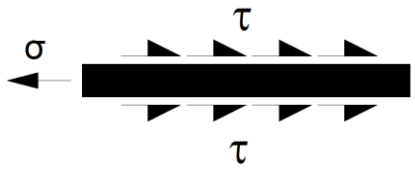

Fig. 4. *Axial stress on sample*

Other roles that the matrix fulfils: protecting the fibres during handling, putting into operation and performing the service, keeping them in positions that remove the risk of cracks, chemical compatibility between it and the fibres, improving the shock and fracture resistance of the composite.

The type of matrix used by us in this experimental work is an epoxy resin. This range of resins is predominantly used in the manufacture of high-performance composites. Considering the purpose and requirements of this experimental work, we need the special mechanical properties that this type of resins offer. In addition, they are resistant to corrosion and the effects of the environment, with good behavior at high temperatures, a fact that facilitates the installation in the structural elements of a construction. Before applying to the fibres, the resin is treated with hardeners according to a specific recipe, which determines the time and conditions in which the resin hardens. The chemical reaction can take place at room temperature or at high temperatures. A great advantage of these resins is the possibility to slow down the hardening process, by subjecting them to lower temperatures than necessary, giving the possibility to create pre-impregnated products, which can later be completed or put into operation. However, it presents disadvantages due to the high cost, the toxicity of the gases resulting from combustion, the high viscosity that complicates the lamination process.

3. Methods and results

In this experimental work we aim to increase the mechanical and physical resistance behavior of certain materials with the help of carbon fiber laminated with epoxy resins. We chose to use as raw material for samples: concrete, solid brick sandwich, wood, and extruded polystyrene. Depending on the utility of each, after lamination with carbon fibres, the samples are tested for bending moment, compression, fire resistance and shock resistance.

3.1. Preparation of samples

For all the samples we used the same technological process, carbon fiber lamination. Their surfaces were cleaned of dust, debris and other foreign bodies. We made sure that the wood is not treated with any kind of chemical substance and the extruded polystyrene was subjected to a test beforehand where we followed its behavior, from a chemical point of view, when it is in contact with the epoxy resin. In the next step, I prepared the resin by adding a specific amount of hardener, which would allow it to harden at ambient temperature. After applying the first layer of resin, on each of the samples, I laid a layer of carbon fiber fabric, cut to

THE ANNALS OF "DUNAREA DE JOS" UNIVERSITY OF GALATI
FASCICLE IX. METALLURGY AND MATERIALS SCIENCE
N°. 3 - 2022, ISSN 2668-4748; e-ISSN 2668-4756
Article DOI: https://doi.org/10.35219/mms.2022.3.08

size, along with another layer of resin, to completely embed the fabric in the resin. For the next layer of carbon fiber, the process is repeated.

We obtained the following samples: extruded polystyrene prisms with the size 10 x 10 x 3 cm: - 1 x laminated with 1 layer of carbon fibres (1); - 1 x laminated with 2 layers of carbon fibres. Firewood samples with the size 1 x 4 x 55 cm: - 2 x laminated with 1 layer of carbon fibres (2); - 2 x laminated with 2 layers of carbon fibres. Solid brick samples, sandwich of 2 half bricks with M5 mortar, final size 12 x 12 x 17: 3 x laminated with 1 carbon fiber layer, (3). Concrete samples: cylinder h = 300 mm, d = 150 mm – 3 x side laminated with carbon fiber (4); - 3 x laminated with carbon fiber strips with a width of 5 cm (5). Prism with size 10 x 10 x 55 laminated with 2 layers of carbon fiber on one side (6). Standard samples are added to each sample category [1-3, 6, 7].

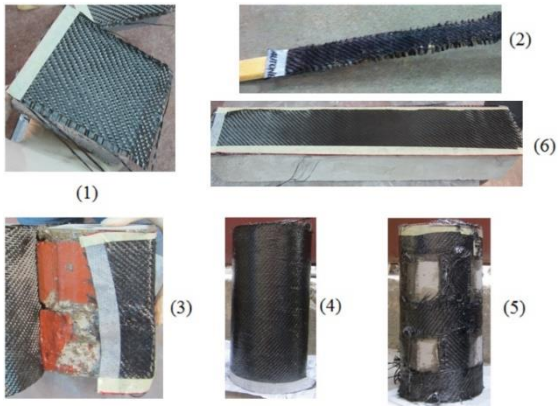

Fig. 5. *Preparation of samples*

3.2. Resistance to fire and shock

Laminated extruded polystyrene samples were tested with an open flame on the laminated side. The result was compared with the standard sample and a sample with glass fiber and special polystyrene adhesive, shown in the adjacent graph. It should be mentioned that in the case of the sample laminated with carbon fiber, burning occurs as in the case of the standard sample, while in the case of the sample covered with adhesive, it burns smoulderingly, without warning signs, which can represent a danger to you.

The shock resistance was determined by free-falling a 0.5 kg metal ball several times from a height of 1 m. No damage was recorded in the structure of the carbon fiber laminated sample.

The classic adhesive sample was destroyed in this test after only two drops of the ball.

Due to the shock resistance, the special appearance, and the fact that carbon fiber can be shaped into any shape, we recommend the use of polystyrene laminated with carbon fiber for special interiors: car showrooms, art galleries etc. [2, 3, 6].

Fig. 6. *Determination on fire resistance*

3.3. Compression resistance

For this test we used the brick samples and the concrete cylinders. After both tests, it was found that fiber lamination increased the strength of both samples. The samples failed when the carbon fiber broke. The standard brick sample yielded at an average value of 15.7 N/mm^2 compared to the fiber-reinforced sample at 17.98 N/mm^2. I calculated the recipe for C16/20 concrete, but the tests resulted in class C18/22.5. The reinforcement with carbon fiber strips increased the strength of the concrete with an average value of 0.80 N/mm^2 even though the reinforcement dosage was not optimal. The samples of reinforced concrete on the entire lateral surface with carbon fibres yielded at the average value of 25.07 N/mm^2. Limited by the small number of samples used, we cannot conclude the increase of the concrete class to C25/30, but all the results obtained fell within this class [2, 3].

3.4. Tensile bending strength

The wooden and concrete prisms were subjected to bending moment. A surprising result in the case of the concrete prism laminated with 2 layers of carbon fibres, where the resistance compared to the standard sample was significantly higher.

The standard prism yielded at 5.17 N/mm^2. The sample yielded at 9.12 N/mm^2 when the adhesion between the fibres and the sample suddenly weakened, a glass fiber resin being used. In the case of wooden prisms, the results are uncertain due to the incompatibility between the samples and the press and the poor adhesion between the resin and the wood. But an improvement in the resistances can be seen even from the approximate results [2, 3].

THE ANNALS OF "DUNAREA DE JOS" UNIVERSITY OF GALATI
FASCICLE IX. METALLURGY AND MATERIALS SCIENCE
Nº. 3 - 2022, ISSN 2668-4748; e-ISSN 2668-4756
Article DOI: https://doi.org/10.35219/mms.2022.3.08

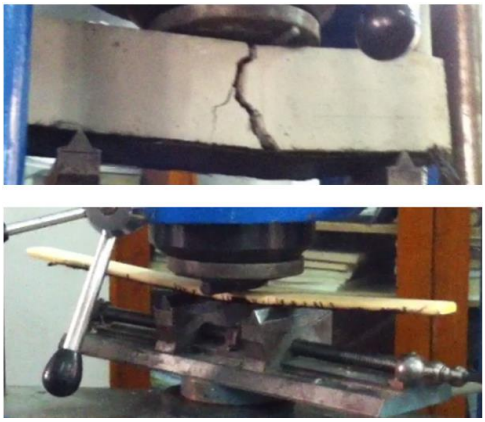

Fig. 7. *Determination on bending strength*

4. Conclusions

Following laboratory tests, it has been reached the following results:

- Polystyrene laminated with carbon fiber has a behavior, in an open flame, different from that covered with glass fiber and classic glue. The laminated one burns with a flame, a fact that will immediately indicate the possibility of a fire, while the one covered with classic adhesive burns smoulderingly and for a long time, behind the adhesive layer, without giving warning signs of fire. In both cases, the time required for the polystyrene to ignite increased significantly.

- The polystyrene laminated with carbon fiber has a significantly higher shock resistance than the one covered with fiberglass and classic adhesive, the latter sample being destroyed during the tests, while the one laminated with carbon fibres did not suffer structural or aesthetic damage.

- In the case of concrete cylinders laminated with carbon fiber, we recorded an increase in compression resistance of 4.03% in the case of those reinforced with carbon fiber strips and of 34.86% in the case of those completely laminated with carbon fiber. The layer of laminated carbon fibres acted as a fret, the samples yielding when it broke, providing no more support to the samples that were already cracked.

- The brick sandwich laminated with carbon fiber behaved similarly to the concrete cylinders, achieving an increase in compressive strength of 14.97%. The failure process is similar to that of cylinders.

- The flexural tension test of the wooden samples laminated with one or more layers of carbon fiber was compromised due to the incompatibility of the sample with the press used. The results obtained are uncertain, but we can state based on them that under favourable conditions the tensile strength by bending will increase significantly. In the laboratory we obtained an increase of 27.78 to 51.36% of the tensile strength by bending.

- The laminated concrete prism with two layers of carbon fiber on the stretched side, recorded a 73.49% increase in tensile strength by bending. It is a surprising result, considering that the sample failed when the adhesion between the laminated layer and the sample was broken. We are confident that when the carbon fiber lamination technology is applied under favourable conditions the samples can acquire better strengths, because if the adhesion is appropriate the samples will yield to the breaking of the carbon fibres, thus the strengths will increase.

In conclusion, the use of composite materials in construction increases the mechanical resistance of the materials. But the technological process of application and lamination must take place in favourable and specific conditions. The results of our tests confirm these two aspects, although we did not manage to reach the maximum potential of this technology.

References

[1]. Daniela Manea, *Materiale Compozite*, UT Press Cluj Napoca, 2003.
[2]. Răzvan Andrei Iernutan, Florin Babota, *Autoclaved Cellular Concrete (ACC) Masonry with Vertical Hollows Confined with Disperse Reinforced Concrete*, Procedia Engineering, vol. 181, p. 300-307, ISSN 1877-7058, 2017.
[3]. Razvan Andrei Iernutan, Florin Babota, Raluca Istoan, *Carbon Fibre Reinforced Aluminium Mesh Composite Materials*, Jurnal Procedia Manufacturing, vol. 32, p. 901-907, 2019.
[4]. Diaconu D., Danescu C., Stoian V., Nagy-Gyorgy T., *Consolidarea grinzilor la forta taietoare folosind materiale compozite*, Sesiunea de comunicari stiintifice, Cluj-Napoca, 2005.
[5]. Ianca S., Nagy-Gyorgy T., Daescu C., *Influenta tehnologiei de reabilitare asupra rigiditatii elementelor de zidarie*, Zilele Academice Timisene, Timisoara, 2007.
[6]. ***, *Panza din fibra de carbon, tesuta, pentru consolidari structural*, SikaWrap® -230C.
[7]. ***, www.compozite.net, accessed: 10.05.2013.

MANUSCRISELE, CĂRŢILE ŞI REVISTELE PENTRU SCHIMB, PRECUM ŞI ORICE CORESPONDENŢE SE VOR TRIMITE PE ADRESA:

MANUSCRIPTS, REVIEWS AND BOOKS FOR EXCHANGE COOPERATION, AS WELL AS ANY CORRESPONDANCE WILL BE MAILED TO:

LES MANUSCRIPTS, LES REVUES ET LES LIVRES POUR L'ECHANGE, TOUT AUSSI QUE LA CORRESPONDANCE SERONT ENVOYES A L'ADRESSE:

MANUSCKRIPTEN, ZIETSCHRITFTEN UND BUCHER FUR AUSTAUCH SOWIE DIE KORRESPONDENZ SID AN FOLGENDE ANSCHRIFT ZU SEDEN:

After the latest evaluation of the journals by the National Center for Science Policy and Scientometrics (**CENAPOSS**), in recognition of its quality and impact at national level, the journal will be included in the B^+ category, 215 code (http://cncsis.gov.ro/userfiles/file/CENAPOSS/Bplus_2011.pdf).

The journal is already indexed in:
DOAJ: https://doaj.org/
SCIPIO-RO: http://www.scipio.ro/web/182206
EBSCO: http://www.ebscohost.com/titleLists/a9h-journals.pdf
Google Academic: https://scholar.google.ro
Index Copernicus: https://journals.indexcopernicus.com
Crossref: https://search.crossref.org/

The papers published in this journal can be viewed on the website: http://www.gup.ugal.ro/ugaljournals/index.php/mms

Name and Address of Publisher:
Contact person: Prof. Dr. Eng. Elena MEREUȚĂ
Galati University Press - GUP
47 Domneasca St., 800008 - Galati, Romania
Phone: +40 336 130139
Fax: +40 236 461353
Email: gup@ugal.ro

Name and Address of Editor:
Ș. L. Dr. Eng. Marius BODOR
"Dunarea de Jos" University of Galati, Faculty of Engineering
111 Domneasca St., 800201 - Galati, Romania
Phone: +40 336 130208
Phone/Fax: +40 336 130283
Email: marius.bodor@ugal.ro

AFFILIATED WITH:

- THE ROMANIAN SOCIETY FOR METALLURGY
- THE ROMANIAN SOCIETY FOR CHEMISTRY
- THE ROMANIAN SOCIETY FOR BIOMATERIALS
- THE ROMANIAN TECHNICAL FOUNDRY SOCIETY
- THE MATERIALS INFORMATION SOCIETY (ASM INTERNATIONAL)

Edited under the care of the FACULTY OF ENGINEERING

Annual subscription (4 issues per year)

Fascicle DOI: https://doi.org/10.35219/mms

Volume DOI: https://doi.org/10.35219/mms.2022.3

Editing date: 15.09.2022
Number of issues: 200
Printed by Galati University Press (accredited by CNCSIS)
47 Domneasca Street, 800008, Galati, Romania